**Response to reviews of manuscript titled: "Effect of vertical wind shear on convective clouds: development, organization, and turbulence."**

Authors: G. Bidou, D. Ricard, and C. Lac

Replies to the reviewers are in blue. Reviewers' comments are in black. Modifications in the main text are in red.

Dear Editor,

We would like to thank the two reviewers for their useful comments and suggestions. As detailed below in the point-to-point answers to the comments of the reviewers, we have addressed all of their comments. In particular, as suggested, we have expanded the references cited in the article to better reflect previous research on the impact of wind shear. We have also enhanced our analysis by including budgets of vertical momentum and cross-sections of TKE within convective cores. In the PDF file containing the changes, additions are shown in blue, and deletions are crossed out in red. We believe that the paper has been significantly improved, and we hope that the revisions satisfactorily address the reviewers's comments.

**Reviewer 1**

General comments:

In this study, a suite of 10 large eddy simulations was performed to explore the sensitivity of vertical wind shear on deep convection evolution. The results are generally consistent with our previous understanding of shear-convection interactions in strongly sheared flows: increased precipitation, larger and fewer cold pools/updrafts, and higher cloud tops through decreased fractional entrainment. While I have no issue with reaffirming the findings of previous studies, it would be nice to have the authors highlight what they believe are novel contributions from this study. In my mind, the main contribution of this paper is the TKE analysis, which I find intriguing for a plethora of reasons. The authors find that up-shear TKE is larger than down-shear TKE, which contrasts with much of the existing literature on shear flow interactions/wake turbulence. Furthermore, I find it surprising that the up/down-shear TKE asymmetry is self-similar, even when transitioning from multicell to supercell modes. I believe there should be some effort to explain "why" the TKE differences exist. This could be done through an analysis of the TKE or vorticity budgets and I believe it would vastly improve the potential impact of the current study. It would also be beneficial to see cross-sections or cloud-edge composites of the TKE to get a better idea for how the TKE varies spatially, since much of the useful information may be lost in the averaging process.

As suggested by the reviewer, we have reiterated in the conclusion section that our results support previous findings regarding the organisation of convection under increasing vertical wind shear. We have also highlighted more recent findings on turbulence and clarified that, as we focus on turbulence within convective cells, our results concerning upstream/downstream turbulence differ from those of other studies that investigate wake turbulence outside convective updrafts.

With regard to this section on turbulence, in addition to the mean vertical profiles, we have included vertical cross-sections of TKE for the control experiment with moderate shear

(W10_S70) (Figure 2) and for the simulation with the strongest shear (W20_S144) (new Figure 6). We have also analysed the vertical momentum budgets as sources of resolved turbulence.

Minor comments:

Lines 24-25: “On the other hand, bending thermals may help trigger and organize deep convection”… This comment requires a citation or at least some explanation of the physical reasoning behind the idea.

The sentence has been removed as the paragraph has been reformulated.

Lines 25-26: “Helfer et al. (2020) shows that both mechanisms operate: shear delays the rise of hot air via thermals and weakens wind velocities, yet remains a necessary condition for sustained deep convection.”… It would be nice to add an explanation/discussion for why shear delays the rise of hot air via thermals and weakens wind velocities. Some literature review of thermal force balance is required.

We have added sentences at the end of this paragraph. “Peter et al, (2019) showed that shear primarily enhances dynamic pressure perturbations. These ones can be interpreted as an aerodynamic lift force due to the shear-driven crossflow (perpendicular to the ascent direction) directed downward, thereby weakening vertical velocities within thermals. Besides, Pastushkov 1975 showed that ambient wind shear can not only inhibit the development of convection and prolong the convective life cycle, but can also intensify convective clouds, depending on the shear intensity. Convective storm intensity can also be expressed in terms of the bulk Richardson number (Moncrieff and Green, 1972, Weisman and Klemp, 1982), which represents the ratio between buoyant energy and wind shear.”

Lines 30-31: “Bending of thermals horizontally may separate the heat source and the updraft core from precipitation resulting from the convection of moist air, preventing cooling of both the heat source and the updraft.”… This is a bit hard to follow. This is explaining the shear-driven tilted updraft that allows for the hydrometeors to not fall directly through the parent updraft, but outside of it, correct?

This is indeed the idea we were trying to convey, this sentence has been rephrased to make it clearer : The tilting of thermals may contribute to the separation between the heat source and the updraft core from precipitation generated by the convection of moist air, thereby preventing the cooling of both the heat source and the updraft through evaporation.

Lines 31-33: It should be mentioned that Helfer et al. (2020) and Helfer and Nuijens (2021) both examine the impacts of vertical wind shear on shallow convection.

It has been clarified that these studies focused on shallow convection.

Lines 36-37: “Entrainment itself is strongly modified under shear : thermals under strong shear conditions entrain environmental air in peculiar ways (LeBel and Markowski, 2023), and convective systems under shear entrain more than their non-sheared counterparts.”…This statement is very vague and latter part of the sentence requires a citation.

We have specified the mechanisms involved (counter-rotating vortex pair) and added some references for the latter part of the sentence (Lasher-Trapp et al., 2021, Morrison et al. 2020; Knupp and Cotton 1985):

"Entrainment itself is strongly modified under shear: thermals developing under strong shear conditions entrain environmental air through a counter-rotating vortex pair mechanism \citep{lebel_analysis_2023}. In addition, convective systems developing under shear entrain more environmental air than their non-sheared counterparts, due to a strengthened overturning thermal circulation (e.g. \citealp{lasher-trapp_entrainment_2021}; \citealp{morrison_confronting_2020}) or through vertical vortices, as in wake entrainment \citep{knupp_convective_1985}."

Lines 38-41: I'm unsure of how this excerpt fits in with the broader discussion. Seems to be misplaced.

As noted by the reviewer, this paragraph was irrelevant to the discussion and has been removed.

Lines 61-62: "As a result, the domain experiences a gradual increase in total energy because surface heating is included but radiative cooling is not. As such, it limits the total simulation time before becoming unrealistic."… How do you determine the time window for which the simulation remains "realistic"?

A first rough estimate (without taking evaporation/condensation into account) of the energy input from the surface fluxes suggests a rise of the domain-mean temperature of ~1,2K over 6 hours. Computing the variation in the average potential temperature for the reference simulation exhibits a raise of 1,6K after 6 hours, the difference being explained by the release of latent heat during condensation.

We consider that the energy of the domain remains reasonable for the 6-hour duration of our simulations, although such a rate would lead to unrealistic conditions if maintained for too long.

Lines 73-75: Doesn't the white noise method also introduce a characteristic scale (it is grid scale noise)?

Unlike the warm bubble method which introduces energy, the white noise averages to a 0K mean temperature variation. Therefore, it is not meant to trigger the convection but to create heterogeneities from which instabilities can appear. As such, we do not believe it would introduce a characteristic size for the convective cells.

We rephrased the paragraph to emphasise this idea : "Convection is triggered using a white-noise perturbation in potential temperature of amplitude 0.2 K within the lowest 1 km. This ensures the loss of horizontal homogeneity required to produce vertical motion, without introducing energy."

Line 149-150: I'm not sure that I fully agree with this statement. This would only be true if entrainment was the only other term in the vertical momentum equation, but as we know, the pressure perturbation dynamics play a major role. In supercells, the upward-directed pressure gradient driven by rotational dynamics cannot be neglected as it is a significant source of vertical momentum. Using the same concept, an overshooting top would imply net detrainment over the course of the parcel's life (not impossible, but something to consider).

The following paragraph relates to the fractional entrainment/detrainment computation, from which we show that fractional detrainment varies little across simulations, unlike entrainment.

The incriminated sentences have been rephrased to suggest rather than assert our hypothesis, and to provide a clearer transition to the next paragraph : This could be caused by the dilution of cold and dry entrained air into the warm and moist air of the updraft, thereby reducing buoyancy. From this understanding, the higher cloud tops in more strongly sheared environments could indicate that their convective cores experience reduced entrainment dilution.

Line 156: correct to bulk-plume

This typo is corrected.

Line 156: “we derive fractional entrainment rates…” … The fractional entrainment rates will not tell you all that much about the actual fluid flow through the cloud interface, given the assumption that you are entraining the mean environmental air. Also, it is mentioned elsewhere in the paper that the convection nearly fills the domain rather quickly and in that case you cannot cleanly partition the “environment”.

We defined environmental air as the air outside the clouds, which remains sufficiently abundant at the updraft altitudes considered here (2-8 km AGL). Convection itself does not fill the entire domain, although the anvil cloud cover does by the end of the simulation, which further justifies limiting the simulations to 6 hours.

Line 159: smoothen —-> smooth

This typo is corrected.

Line 184: asymetry —-> asymmetry

This typo is corrected.

Lines 191-196: Maybe this is already what is being referred to, but the increased TKE could also be associated with the thermals interacting with the mean flow, acting as obstacles, although this can also produce wake turbulence on the down-shear side (Malkus, 1949; Heymsfield et al., 1979; Kingsmill and Wakimoto, 1991; McMichael et al., 2022; LeBel and Markowski, 2023).

Interestingly, in shallow convection studies, the TKE enhancement is seen on the down-shear side (Gu et al., 2021; McMichael et al., 2022), with organized entrainment occurring on the up-shear side (McMichael et al., 2022). It’s possible that the wake-related TKE enhancement on the down-shear side is outside of the plume core examined in the paper. It also seems conceivable that the much larger shear magnitudes in deep convection are creating more pronounced obstacle effects, especially on the up-shear side in supercells. Or perhaps, there are some vorticity processes (stretching/tilting) related to the mesocyclone.

This idea of a turbulent wake has been mentioned during the writing process, and we believe that this would indeed develop outside the « core plumes » considered in our study, and would therefore not contradict our results.

To confirm the presence of turbulent wakes, we examined horizontal cross-sections of column-averaged TKE (see following figure). These show the presence of predominantly subgrid TKE downwind of the convective cores, confirming the existence of turbulent wakes. However, these wakes appear to be less turbulence-intensive than the updraft cores themselves.

We therefore added references to turbulent wakes, together with relevant citations, in both the introduction and the conclusion of this section of the text. The following sentence was added to the introduction: A first indication of such an asymmetry was reported by Malkus, 1949, who highlighted stronger turbulent motions upwind of cumulus clouds and downwind of cumulonimbus clouds within a turbulent wake.

The following discussion was also added to the conclusion of the section: This difference in TKE may appear inconsistent with the concept of a turbulent wake generated by convective cores acting as obstacles to the mean flow (Malkus, 1949 and Kingsmill, 1991). However, because our analysis focuses on the updraft cores (as seen in Figure \ref{fig:vertical_slices_W10_S70} e) and f), potential wake regions may have been excluded, thereby allowing the detection of enhanced upwind TKE within the convective cores themselves. Vertical (Figures 2 e-f, 6 e-f) and horizontal (not shown) cross-sections of TKE nevertheless confirm the presence of a turbulent wake downwind of the convective cores, mainly in the subgrid TKE field, although this wake appears less turbulent than the updraft cores.

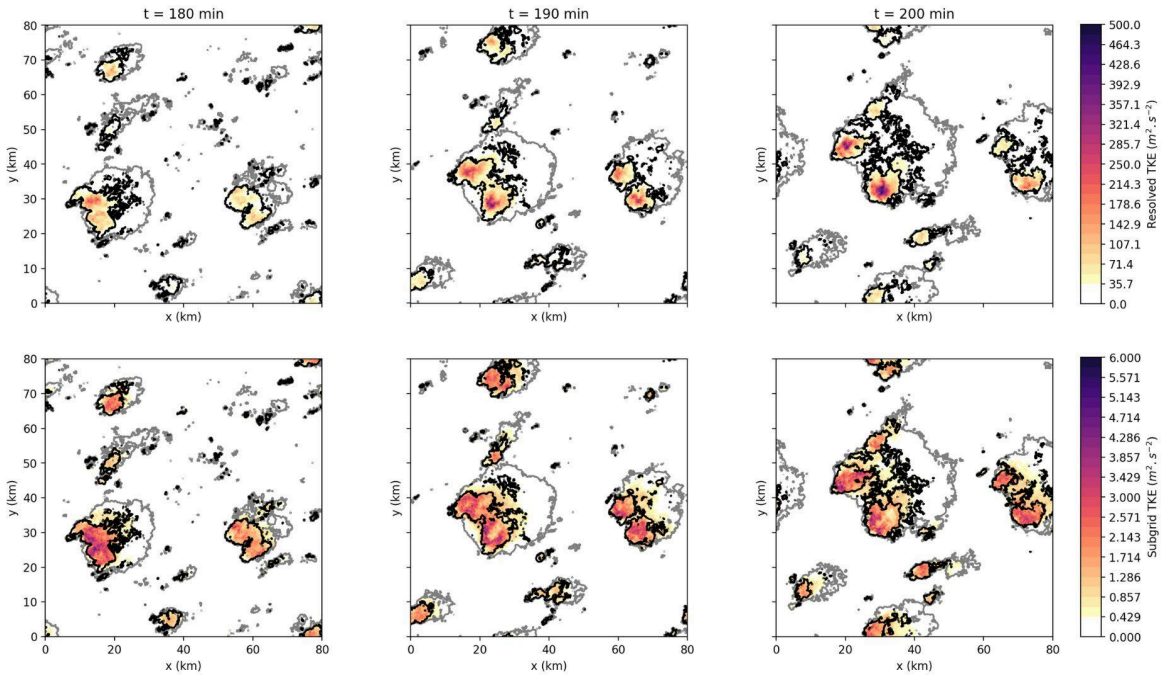


Column-averaged TKE for simulation W20_S144 at 180, 190 and 200 minutes. First row : Resolved TKE, second row : Subgrid TKE. Grey contour : clouds, black contour : convective cores.

(this figure was not added to the draft)

Line 229: “verifying this requires to quantify objectively this organization”… I suggest a rewording.

The introductory sentences to this section were reworded as follows : We hypothesise that many of the differences between our simulations can be related to differences in convective organisation. We therefore attempt to measure such differences.

Line 242: The four indicators need to at least be briefly described within the paper, as they are not overly common indicators.

We added a brief description of the four metrics used as follows : These four indicators are: cloud-top altitude standard deviation, characteristic length, void size ratio (the ratio between the largest cloud-less rectangle in the domain and the domain size), and directional alignment, which we interpret here as eccentricity.

Line 247: Tendencies appear on these graphs. —> Needs a figure reference.

This sentence was indeed unclear, we rephrased it as such: A trend toward greater organisation with increasing shear appears in these graphs (Figure \ref{fig:janssens} a - c)

Line 270-271: It is also consistent with increased upward-directed pressure perturbation gradient force driven by the rotating updraft. It would be nice to see some vertical momentum budgets to quantify some of these qualitative statements.

We added the following figure with vertical momentum budgets (Figure 8) with some comments in sections 3.1 and 3.2)

Line 287: kinetical —> kinetic

This typo is corrected.

Minor aesthetic point: Figures 4, 8, 9, 13 seem to have lower image quality than the other figures.

Quality of figures 8 and 9 improved

References:

Gu, J.-F., Plant, R.S., Holloway, C.E. & Jones, T.R., 2021: Composited structure of non-precipitating shallow cumulus clouds. Q J R Meteorol Soc, 147: 2818–2833, https://doi.org/10.1002/qj.4101.

Heymsfield, A. J., P. N. Johnson, and J. E. Dye, 1978: Observations of moist adiabatic ascent in northeast Colorado cumulus congestus clouds. J. Atmos. Sci., 35, 1689–1703, https://doi. org/10.1175/1520-0469(1978)035,1689:OOMAAI.2.0.CO;2.

Kingsmill, D. E., and R. M. Wakimoto, 1991: Kinematic, Dynamic, and Thermodynamic Analysis of a Weakly Sheared Severe Thunderstorm over Northern Alabama. Mon. Wea. Rev., 119, 262–297, https://doi.org/10.1175/1520-0493(1991)119<0262:KDATAO>2.0.CO;2.

Malkus, J. S., 1949: Effects of wind shear on some aspects of convection. Eos, Trans. Amer. Geophys. Union, 30, 19–25, https://doi.org/10.1029/TR030i001p00019.

McMichael, L. A., D. B. Mechem, and T. Heus, 2022: Shallow Cumulus Entrainment Dynamics in a Sheared Environment. J. Atmos. Sci., 79, 3275–3295, https://doi.org/10.1175/JAS-D-22-0062.1.

**Reviewer 2**

Review of Bidou et al, ACP, 23/02/26

This study investigates the effect of low-level wind shear on characteristics of deep convection by using a set of LES experiments initialised with different mean wind profiles.

Strengthened low-level shear is shown to have a positive feedback on multiple measures of convective intensity. The overall tone of the article is primarily descriptive: as the authors themselves state (L284), they “mainly [focus] on different diagnostics of convection rather than deeply analysing the physical mechanisms”. This is perfectly acceptable – however, my primary criticism of the article is that this topic has been explored extensively in the literature, with similar LES studies stretching back to at least the 1980s. The present article acts as a coherent review and demonstration of known mechanisms in a single setting; however, it does a generally poor job of appropriately referencing prior work and identifying the analysis here that is novel. My impression is that only the TKE results are novel. A thorough literature review, and clearly-identified discrimination between known and new findings, are both required to make this article suitable for publication. I recommend at least Major revisions be undertaken.

Major comments

Literature review:

Essential prior literature in this field, particularly regarding work from the present decade, is either missing or not cited extensively enough. In general, the article feels a little outdated in its implicit knowledge of the field, ignoring important modern development and context. That several such papers have come from French groups which are also part of CNRS makes this all the more baffling! A thorough review away from the article is required, which should then be translated into a more complete Introduction and Conclusions, and improved references for findings that are re-affirmed in the Results section. Here are some key elements to work on:

• Effect of low-level shear on entrainment. On L160 the authors end their analysis of Fig. 6 by stating “This is consistent with the previous hypothesis of shear reducing entrainment dilution of the convective cores”. This hypothesis was first posed, and verified in LES simulations, by Mulholland et al, JAS (2021). It has further been verified in km-scale explicit simulations (Maybee et al, GRL (2024) & QJRMS (2025)).

Some of these articles are cited, however not for this key physical mechanism. The Mulholland paper, in particular [I am not an author], uses a very similar framework to this article, varying initial state shear for a set of LES experiments, to rigorously investigate the relationship between entrainment, shear and convective intensity.

This must be much more clearly acknowledged throughout this article.

The hypothesis and the associated references have been clarified and more explicitly cited, both in the introduction : Another hypothesis is that tilting of thermals broadens the updraft, reducing the dissipating effect of the entrainment of cold, dry air into the updraft. This mechanism was proposed by Mulholland, 2021 in a study of LES of squall-lines and has been further explored using km-scale simulations (Abramian, 2023; Maybee, 2024 and Maybee, 2025).

and in the relevant result paragraph :

This is consistent with the hypothesis from Mulholland, 2021, namely that shear reduces entrainment dilution within convective cores, as well as with the findings of Abramian, 2023 regarding the effect of shear-modulated entrainment on precipitation.

• I was very surprised, and disappointed, to find that the authors have neglected recent articles [with which I was not involved] led by Sophie Abramian from the group at the Laboratoire de Météorologie Dynamique; in particular, Abramian et al, GRL (2021); and Abramian et al, JAMES (2023). These papers use LES simulations to verify physical hypotheses regarding the orientation of squall lines relative to low-level shear, and the contribution of shear-modulated dynamical controls (entrainment) to changes in extreme rainfall in increasing-shear environments.

A mention of those articles has been added in both entrainment and cold pool sections (see previous comment).

• The authors do make reference to some theories for understanding the role of shear in convective organisation, such as the classic RKW theory. They have neglected a more recent key theory whereby shear modulates the low-level inflow into convective systems and thereby convective characteristics (Alfaro, JAS (2017)). This theory offers testable metrics relating to maximum updraft velocities and precipitation; its predictions were independently tested in LES experiments initialised from observed soundings by Bickle et al, JAS (2022). It would be particularly interesting to consider an analysis of the Alfaro metrics in the context of the different up/downstream TKE values.

A mention to this theory and associated metrics have been added to the discussion with the relevant citations : Our evolution of the organisation relies on three metrics. Although Janssens, 2021 showed that these are fairly representative of several others, we could also have used other commonly employed metrics such as I_org, or more recent ones such as those based on the layer-lifting model of convection (Alfaro, 2017), which have been used to evaluate squall lines in LES studies (Bickle, 2022).

• There is now an extensive body of literature surrounding shear controls on deep convection in satellite observations/reanalysis and km-scale convection permitting models. Such work provides an important motivation for the kinds of experiments conducted in this article, since they can inform understanding of new modelling systems or observations. Some reference to this context would improve the Introduction and its motivation of the article. Consider e.g. Klein et al, ERL (2021); Chen et al, GRL (2023); Maybee et al, GRL (2024); Muetzelfeldt et al, JAS (2025). And from CNRS, Roca et al, JGR-A (2025)!

Article motivation has been strengthened by the inclusion of satellite observations and reanalysis studies : Moreover, recent satellite observations and reanalysis have shown that wind shear correlates weakly with other environmental factors (Chen, 2023), but has a significant effect on convective organisation and precipitation (Muetzelfeldt, 2025).

Supercells:

The authors describe the high shear experiments (W20_S144 and W15_S106) as generating supercells. How have the systems been diagnosed as supercells? I see no presentation of quantitative evidence that suggests supercells, with Fig. 5 showing systems simply with coherent organised updrafts. As stated in Markowski and Richardson (2011), "…consensus now seems to favor a dynamical criterion in place of a longevity criterion for classification of a storm as a supercell. The widely accepted dynamical criterion is the presence of a persistent, deep mesocyclone within the updraft. A mesocyclone is a region of vertical vorticity with a characteristic width of 3–8km and magnitude of O(10−2) s−1."

Please could the authors demonstrate that the storms labelled as supercells meet such a dynamical criterion? If a deep mesocyclone cannot be detected or demonstrated in these systems, I would ask that all references to supercells be removed from the article.

This is a very pertinent remark, as we did not explicitly demonstrate that the systems we observed were indeed supercells. Below, we list several analyses used to assess the validity of this terminology.

We computed vertical vorticity, as requested by the reviewer, and found that the updrafts in the high-shear experiments do indeed exhibit vorticity values exceeding $10^{-2}$ $s^{-1}$. We have added a black contour indicating this threshold in figure 5.

We also added vertical cross-sections of a representative convective cell from simulation W20_S144, highlighting a broad (within the 3-8 km characteristic width) and vertically coherent updraft reminiscent of supercell structures, in contrast to the behaviour shown in figure 2.

The computation of updraft helicity (figure 4 panel b) shows a pronounced peak around 200 minutes in the two strongest-shear simulations. Additional horizontal cross-sections of this metric (not shown in the draft) indicate that it is concentrated within the updraft regions.

Finally, we verified that the trajectories of the identified storms are deflected relative to the mean wind direction starting after the storm-splitting process, which is not observed for the storms in the other simulations (also not shown in the draft).

We believe that these elements are sufficient to support the classification of these storms as supercells, and we have therefore retained this terminology in the article.

Analysis methods:

The present article does include a Methodology section, which describes the MesoNH model and the experiments that form the data for the paper.

However, no details are given of any of the analysis methods used throughout the Results section. This undermines much of the Results section, as the nature of what is being shown is ambiguous. In particular, details should be provided regarding:

• Identification of updraft cores. Is there an area threshold on a contiguous ascending domain at a set level, is this all w>0 points, etc? I cannot fully interpret some figures as I am unclear on this point.

This point was indeed not clearly stated. We have added the definitions used for our diagnostics : A grid point is classified as cloudy when the mixing ratio of cloud hydrometeors (the sum of cloud water and cloud ice) exceeds 1.10^-6 kg/kg. A grid point is classified as part of an updraft core when it satisfies both the cloudy condition and a local vertical velocity exceeding 2 m.s^-1

• Entrainment profile calculations. The bulk plume method mentioned in context of Fig.6 should be briefly described, explicitly highlighting the key technical details which underpin the Results. It was disappointing to have this relegated to a citation when these results play an important role.

A definition of the method used was indeed missing in the main text, this has now been corrected : The bulk-plume method for offline computation, as described in Siebesma et al. (2003) and Dauhut et al. (2015), is based on the assumption of a single, uniform

updraft plume embedded in a homogeneous environment. The vertical variation of conservative variables within the plume is therefore entirely due to mixing between environmental and updraft air.

• Organisation indices and 2D cloud masks. How exactly are these calculated? What are “void sizes”?

I note that some details here may be in the appendices. Please move them to the main text so that readers do not need to refer to appendices, these methodological details are important for interpretation of the results.

The “void size ratio” metric is not commonly used, as it was only recently introduced by Janssens et al (2021). We have added a description to the text: the ratio between the largest cloud-less rectangle in the domain and the domain size

We have also moved a short definition of the 2D cloud masks from the appendices to the main text to make the methodology more explicit: we derived 2D cloud masks from our 3D fields by classifying a model column as "cloudy" when at least 30 grid points within the column exceed the 1.10^-6 kg/kg threshold

Other comments

• L21 “all studies agree on this” – this language is quite loose, and some studies do not agree on the effect of shear on rainfall. I suggest rewording.

We rephrased the sentence as follows to highlight that studies using different methods find similar results : varied studies agree on this

• L35 “Entrainment itself is strongly modified under shear” – important missing citation, Mulholland et al, JAS (2021), see Major comments.

Citation added to the text

• Introduction – missing references as in Major comments. But also, I was surprised that no mention is made as to the relationship of shear to observed species of deep convection and their organisation. In particular, where do Mesoscale Convective Systems, the archetypes of organised convection and shear beneficiaries, fit in?

As suggested by the reviewer, we have added references in the introduction and inthe following paragraph on the relationship between wind shear and the organisation of deep convection.

The organisation, development, and maintenance of Mesoscale Convective Systems (MCSs) are governed by the three primary ingredients for deep moist convection (moisture, lift, and instability), as well as by the way vertical wind shear interacts with convective updrafts and cold pools (Schumacher and Rasmussen, 2020; Markowski and Richardson, 2010). Under weak wind shear conditions, convection is poorly organised and consists of isolated cells. Multicellular systems are favoured under weak to moderate shear, whereas supercells develop under strong shear conditions, particularly when there is directional shear in the wind profile (e.g. Rotunno et al, 1985, Weisman et al, 1988).

• Section 2.2 – It may be worth highlighting your experiment naming convection explicitly to the reader? While reading the results it took me a little while to twig that the labels display the mean winds and shear for each experiment.

Mention of the naming convention has been added in the text.

• Figure 3/L107 – See Major comment; how did you identify “updraft cores”?

As stated in the major comment above, this point was indeed not clearly stated, we added the definition that we used for our diagnostics.

• L117 “those two” – too informal and clear, please state the experiments explicitly.

This formulation has been changed to explicitly name the two simulations in question

• L119-120 “producing a few large updraft cores with very strong vertical velocities….These supercells correspond to the maxima shown in…” – see Major comment, how have you diagnosed the systems as supercells? Where is the evidence of strong vertical vorticity?

As stated in the major comment above, this is a very pertinent remark, as we did not explicitly demonstrate that the systems we observed were indeed supercells. Several diagnostics have been performed to assess the presence of supercells, some of which have been added to the article.

• Fig. 6b – please reformat the correlation values, this many decimal places is entirely meaningless. I suggest 2s.f. The Figure caption should really be more detailed in describing how the lines/r^2 values relate to the marker shapes, too.

Thank you for the remark, the significant values in the legend were indeed mis placed. We have therefore limited the labels to two significant digits.

The legend has also been reorganised to make it clearer which $r^2$ corresponds to which marker.

• L156 – Correct “bulk plum” -> “bulk plume”. More importantly, I am not familiar the method for computing the provided entrainment/detrainment profiles and as a general reader would expect such detail to be provided. See Major comment.

This typo is corrected.

As stated in the major comment above, a definition of the method used was indeed missing in the main text, this has been corrected.

• L193-194 “Shear may cause the environmental wind to exceed the storm motion, which could explain a higher TKE upstream of the convective cores” – See Major comment, please discuss this in the context of the theory of shear modulated of low-layer inflow posed by Alfaro, JAS (2017).

As stated in the major comment above, we added a mention to this theory and the associated metrics with the relevant citations.

• Figure 11 – The caption only describes a single line in the top plot of each panel. What is the bottom line plot? And what are the different lines within each plot? The figure looks very pretty, but it’s extremely hard to pull a concrete scientific message out of. The panels are also quite similar between simulations. I would strongly suggest finding a better method to display this information; my suggestion would be box or violin plots, which will being less aesthetic are more quantitative. You could group different experiments’ distributions at common timesteps, and choose six key timesteps, to convey the same data but in a clearer form.

This figure has been changed. After a few uncompelling trials with violin plots, we elected to keep the current form, but simplified to hopefully represent the information more accurately. The plots for the mean and median have been removed; they remain in Figure 12. We reduced the amount of plotted distributions, keeping only one out of three to improve visibility.

The caption has been corrected to convey more precisely a description of the figure.

• L216/Fig. 12 – What exactly is being plotted here? By context it is the same as Fig. 11, which is virtual potential temperature in the first vertical level, which is not the same as the surface. Yet the text refers to “cool[ing] the surface more efficiently”. The first vertical level is not the same as the surface? Are you plotting surface or skin temperatures?

The plotted data is on the first model level, text and caption corrected accordingly.

• L230 – suggest adding Biagioli and Tompkins, JAS (2023) to reference list regarding difficulties of quantifying organisation.

Relevant reference added and mentioned in the text

• L244 “we derived 2D cloud masks from our 3D fields” – see Major comment; how?

As stated in the major comment above, we moved the description of the method used from the appendix to the main text.

• L247 “Tendencies appear on these graphs” – suggest removing and rewriting this sentence, as it is extremely unclear what meaning is being conveyed.

This sentence was indeed unclear, we rephrased it as such: A trend of higher organisation with stronger shear appears on these graphs.

• L249 – See Major comment; what are void sizes? You must be more detailed when introducing new methods and metrics.

As stated in the major comment above, a definition of the method used was indeed missing in the main text, this has been corrected.

• Fig. 14d – I strongly recommend removing this panel, it serves no purpose beyond showing that an arbitrarily chosen metric conveys little information, and thus detracts from the rest of the figure. If you wanted to replace the panel, maybe the closest thing to a “single indicator of organisation” (L240) in the sense of its position as a standard metric is Iorg (Tompkins and Semie, JAMES (2017)). There are many issues with this metric, however it is designed for and frequently used in LES settings such as your own. Plotting this could be a nice way of providing a clearer panel that should synthesise information conveyed in the other three.

This panel and metric were, as noted by the reviewer, irrelevant to the discussion and we have removed them to simplify this figure.

# Effect of vertical wind shear on convective clouds: development, organization, and turbulence.

Gaston Bidou[1], Didier Ricard[1], and Christine Lac[1]

[1]CNRM, Université de Toulouse, Météo-France, CNRS, Toulouse, France

**Correspondence:** Gaston Bidou (gaston.bidou@meteo.fr) and Didier Ricard (ricard.didier@meteo.fr)

**Abstract.**

This study investigates the influence of vertical wind shear (hereafter "shear") on deep convective clouds. Using a set of high-resolution Large-Eddy Simulations (LES) produced with the research model Meso-NH and spanning a range of shear intensities, we analyse how variations in shear affect storm organisation and intensity. As shear increases, storms exhibit stronger precipitation, more vigorous updrafts, and more intense cold pools beneath the convective cells. When the shear becomes sufficiently strong, the convective cells evolve into supercells, drastically changing the storm regime and highlighting a non-linearity in the behaviour of convective systems. Turbulent quantities are also affected, with higher subgrid and resolved turbulent kinetic energy (TKE) for stronger storms. Moreover, inside convective cores, upwind TKE exceeds downwind TKE, although the ratio of subgrid to total TKE remains unchanged across simulations. Using four different organisation metrics, a robust increase in convective organisation is diagnosed with increasing shear, with the supercell regime diverging from the other simulations. Vertical wind shear, through its effect on convective organisation, significantly modifies the characteristics of deep convective storms, and should therefore be taken into account in convective parametrisation schemes.

## 1 Introduction

Convective storms are a major source of high-impact precipitation events (Doswell, 2001), and their frequency is expected to increase under anthropogenic climate change (Tippett et al., 2015; Prein et al., 2017; Peleg et al., 2025). Accurately forecasting convective storms and the associated phenomena remains challenging, not only because of the variety and complexity of elements, such as hail (Lac, 2014) and lightning strikes (Goodman and MacGorman, 1986; Mazur and Rust, 1983), but also because convective systems are highly sensitive to their environment (Kirkpatrick et al., 2007).

It is well established that vertical wind shear plays a crucial role in organising deep convection. From the pioneering numerical simulations of Weisman and Klemp, 1982 (hereafter WK82) to the Thompson et al., 2007 data reanalysis and the modelling study of Coffer and Parker, 2015, ~~all~~ varied studies agree on this. The organisation, development, and maintenance of Mesoscale Convective Systems (MCSs) are governed by the three primary ingredients for deep moist convection (moisture, lift and instability) , as well as by the way vertical wind shear interacts with convective updrafts and cold pools (Schumacher and Rasmussen, 2020 ; Markowski and Richardson, 2001). Under weak wind shear conditions, convection is poorly organised and consists of isolated cells. Multicellular systems are favoured under weak to moderate shears, whereas supercells develop under strong shear

conditions, particularly when there is directional shear in the wind profile (e.g. Rotunno and Klemp, 1985; Weisman et al., 1988 ). Moreover, recent satellite observations and reanalysis have shown that wind shear correlates weakly with other environmental factors (Chen et al., 2023), but has a significant effect on convective organisation and precipitation (Muetzelfeldt et al., 2025) . Detailed simulation-based studies have shown that wind shear encompasses several parameters, with distinct effects on convective storms (Peters et al., 2022a). However, its influence on convection initiation, and its more subtle effects during the developing and mature phases still require quantitative assessment.

During the initiation phase, several mechanisms have been proposed. On the one hand, wind shear ~~bends~~ tilts thermals, reducing vertical velocities (Peters et al., 2019) and potentially inhibiting convection initiation ~~. On the other, bending the thermals may help trigger and organise deep convection. Helfer et al., 2020 shows that both~~ (Pastushkov, 1975). Helfer et al., 2020 showed that two mechanisms operate: shear delays the rise of hot air via thermals and weakens initial vertical wind velocities, yet remains a necessary condition for sustained deep convection. Peters et al. (2019) showed that shear primarily enhances dynamic pressure perturbations., which can be interpreted as an aerodynamic lift force associated with shear-driven crossflow directed downward, thereby weakening vertical velocities within thermals. In addition, Pastushkov (1975) showed that ambient wind shear can not only inhibit the development of convection and prolong the convective life cycle, but can also intensify convective clouds, depending on the shear intensity. Convective storm intensity can also be expressed in terms of the bulk Richardson number (Moncrieff and Green, 1972; WK82), which represents the ratio between buoyant energy and wind shear.

Entrainment itself is strongly modified under shear: thermals developing under strong shear conditions entrain environmental air through a counter-rotating vortex pair mechanism (LeBel and Markowski, 2023). In addition, convective systems developing under shear entrain more environmental air than their non-sheared counterparts, due to a strengthened overturning thermal circulation (e.g. Lasher-Trapp et al., 2021; Morrison et al., 2020) or through vertical vortices, as in wake entrainment (Knupp and Cotton, 19 .

During the developing and mature phases, low-level wind shear strongly influences storm motion (Klemp and Wilhelmson, 1978; Rotunno and Klemp, 1982; Weisman and Klemp, 1984; Peters et al., 2020). Several hypotheses have been proposed to explain how shear organises deep convection.

~~Bending of thermals horizontally may separate the~~ The tilting of thermals may contribute to the separation between the heat source and the updraft core from precipitation ~~resulting from~~ generated by the convection of moist air, ~~preventing~~ thereby preventing the cooling of both the heat source and the updraft through evaporation. Helfer et al., 2020 and Helfer and Nuijens, 2021 compared shallow convection simulations with and without shear, as well as under "backward shear" conditions, and confirmed that without proper vertical wind shear, precipitation falls into or upwind of the updraft, leading to weaker convective fluxes.

Another hypothesis is that ~~bending of thermals broaden~~ tilting of thermals broadens the updraft, reducing the dissipating effect of the entrainment of cold, dry air into the updraft. ~~Entrainment itself is strongly modified under shear : thermals under strong-shear conditions entrain environmental air in specific ways (LeBel and Markowski, 2023), and convective systems subjected to shear entrain more environmental air than their non-sheared counterparts.~~

~~Helfer and Nuijens (2021) further showed that excessively strong shear can inhibit the development of secondary convective updrafts triggered by cold pools. This "successive feeding" mechanism , whereby new convective cells develop from the remnants of previous ones, was studied by Misumi et al., 1994. One notable consequence is the systematic upwind tilting of subsequent convective structures~~This mechanism was proposed by Mulholland et al. (2021) in a study of LES of squall-lines and has been further explored using km-scale simulations (Abramian et al., 2023, Maybee et al., 2024 and Maybee et al., 2025 ).

In this study, we investigate how vertical wind shear ~~influence~~ influences both the initiation and development of deep convective clouds using a set of high-resolution Large-Eddy Simulations (LES) produced with the research model Meso-NH with varying shear. Emerging relationships between shear magnitude and the organisation and intensity of the convective systems are examined.

Section 2 describes the model configuration and dataset. Section 3 presents the diagnostics performed, and the trends they unveil. Those are grouped by themes, first on the characteristics of convection, then on turbulent kinetic energy (TKE), and finally on cold pools and organisation. Section 4 summarises and discusses the results.

## 2 Methodology

### 2.1 Model

The simulations are performed with the Meso-NH model (Lac et al., 2018), initially developed by CNRM and the Laboratoire d'Aérologie as a research model for simulating atmospheric phenomena from the meso-scale to the microscale. It solves the anelastic formulation of the pseudo-incompressible system of Durran (1989) to filter acoustic waves. Spatial discretisation relies on the Arakawa C-grid. Time integration used in this study is the explicit 4th-order centered Runge-Kutta (RKC4) associated with a 4th-order centered advection scheme. The microphysics scheme is the one-moment ICE3 scheme (Pinty and Jabouille, 1998). It represents 5 prognostic hydrometeors (cloud water, cloud ice, rain, snow, and graupel). Turbulence is parameterised using a 1.5-order closure (Cuxart et al., 2000), i.e. with a prognostic equation for TKE. In LES mode, turbulence is 3D, taking into account horizontal turbulent fluxes, and the mixing length is determined by the mesh size and stability criteria following Deardorff (1980). No shallow convection scheme is used since convective structures are explicitly resolved at LES resolution.

Radiative processes are omitted in order to isolate shear effects. This also contributes to reduce computational and environmental costs (Appendix C). As a result, the domain experiences a gradual increase in total energy because surface heating is included but radiative cooling is not. As such, it limits the total simulation time before becoming unrealistic, but this is still reasonable for simulations lasting 6 hours (less than a 2-degree increase).

### 2.2 Data

We have carried out large eddy simulations of deep convection in idealised situations. The domain is an 80-kilometre square with cyclic lateral boundary conditions. Following Strauss et al. (2019), the grid spacing is 50 m in the horizontal. The vertical resolution is 50 m up to 13 km above ground level (AGL) then a smooth stretching is applied until 20 km, yielding a total of 292 vertical levels. The time step ranges from 1 to 0.75 s, depending on maximum wind speed, to satisfy the CFL condition. Each simulation is run for 6 hours.

Initial thermodynamic profiles are taken from the analytical vertical profiles of WK82, with a constant mixing ratio of water vapour in the boundary layer (0.012 kg/kg). Surface fluxes are prescribed, constant and spatially uniform, with 200 $\mathrm{W/m^2}$ for sensible heat and 350 $\mathrm{W/m^2}$ for latent heat.

Convection is triggered using a white-noise perturbation in potential temperature of amplitude 0.2 K within the lowest 1 km. This ensures the loss of ~~stability required to initiate convective motion~~horizontal homogeneity required to produce vertical motion, without introducing energy. Another way of initiating convection would be to introduce a warm bubble near the surface, as done by Verrelle et al., 2015 and LeBel and Markowski, 2023, however we fear this may introduce a characteristic size for convective systems, and avoided this method.

Ten simulations were performed, detailed in table 1, differing only in their initial wind speed profiles. Wind shear was prescribed using quarter-circle hodographs with different horizontal wind magnitudes, from 0 to 20 $\mathrm{m.s^{-1}}$, and shear-layer depths, from 0-1 km to 0-3 km (Figure 1 a). The combination of those two parameters was summarised into a single metric to characterise each simulation : the 0-6 km mean wind shear as a proxy for the bulk Richardson number, since the initial CAPE is constant across experiments. Simulations are named to label both the maximum wind speed and the mean shear. Note that one simulation (W0_S0) is run without wind, and another (W10_S0) without shear, with a 10 $m.s^{-1}$ wind, considered as an advection of shear-free environment.

| Simulation | Wind speed ($m.s^{-1}$) | Mean shear ($m.s^{-1}.km^{-1}$) |
|---|---|---|
| W0_S0 | 0 | 0 |
| W10_S0 | 10 | 0 |
| W5_S34 | 5 | 3.4 |
| W7_S49 | 7 | 4.9 |
| W10_S63 | 10 | 6.3 |
| W10_S70 | 10 | 7.0 |
| W10_S72 | 10 | 7.2 |
| W12_S86 | 12 | 8.6 |
| W15_S106 | 15 | 10.6 |
| W20_S144 | 20 | 14.4 |

**Table 1.** Wind speed and shear per simulation

No forcing is imposed to the wind speed, meaning that the environmental wind is free to evolve during the simulation. This causes an evolution of the mean shear over time, as the kinetic energy feeding the storms is progressively depleted (Figure 1 c). Indeed, the mean shear decreases in all sheared simulations. In contrast, the mean shear in the "advection" simulation W10_S0 increases with time due to surface friction reducing wind speed in the lowest vertical levels.

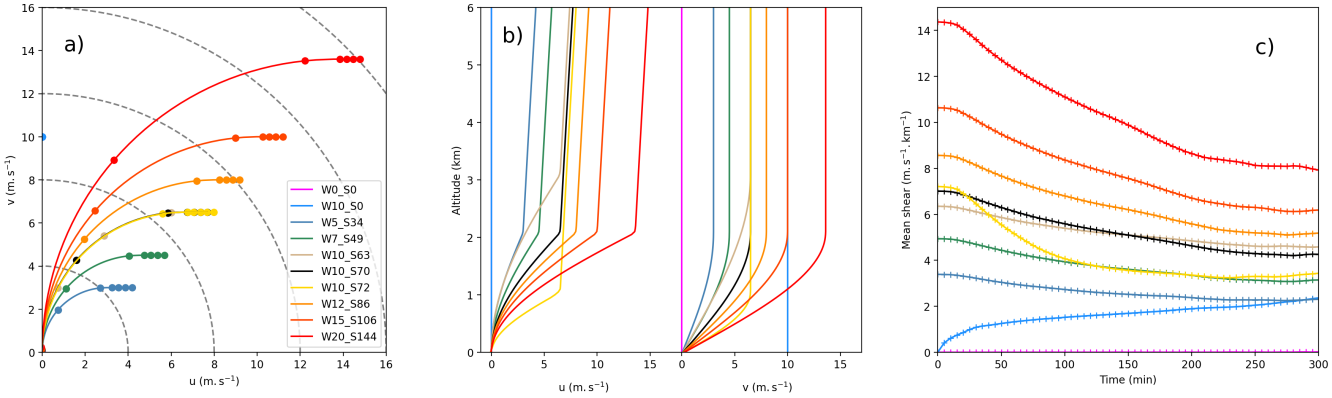


**Figure 1.** a) Hodographs at the initial conditions, b) horizontal wind components at the initial conditions and c) evolution of mean shear over time for all simulations.

## 3 Results

In this section, we identify the key differences between the simulations and analyse how various diagnostics respond to changes in mean shear.

### 3.1 Characteristics of the simulated deep convection

Convective structures develop in all simulations. After 5 hours, cumulonimbus clouds reaching up to 12 km AGL are present. This is confirmed by vertical cross sections of clouds, such as the one in Figure ??2. It is extracted from the reference simulation at 300 minutes (see dashed line in Figure 3d), and shows a deep convective cloud, extending from 2 to 12 km AGL. A convective core is clearly present, with updraft velocities reaching 30 $\mathrm{m.s^{-1}}$, and compensating subsidence in the anvil and around the ascending core. Non-precipitating hydrometeor contents confirm that it is a mixed-phase cloud composed of both liquid water and ice. Note that the liquid part extends higher within the updraft, likely due to temperature anomalies or to supercooled water. Precipitating hydrometeors are also present: rain within and below the updraft, and snow and graupel at higher levels. Graupel mixing ratios are substantial, as expected from the ICE3 microphysics scheme (Lascaux et al., 2006).

Overall, the simulated structures are consistent with LES of deep convective clouds, with explicit circulation within the clouds and well-defined cumuliform structures. This validates our approach and motivates further analysis.

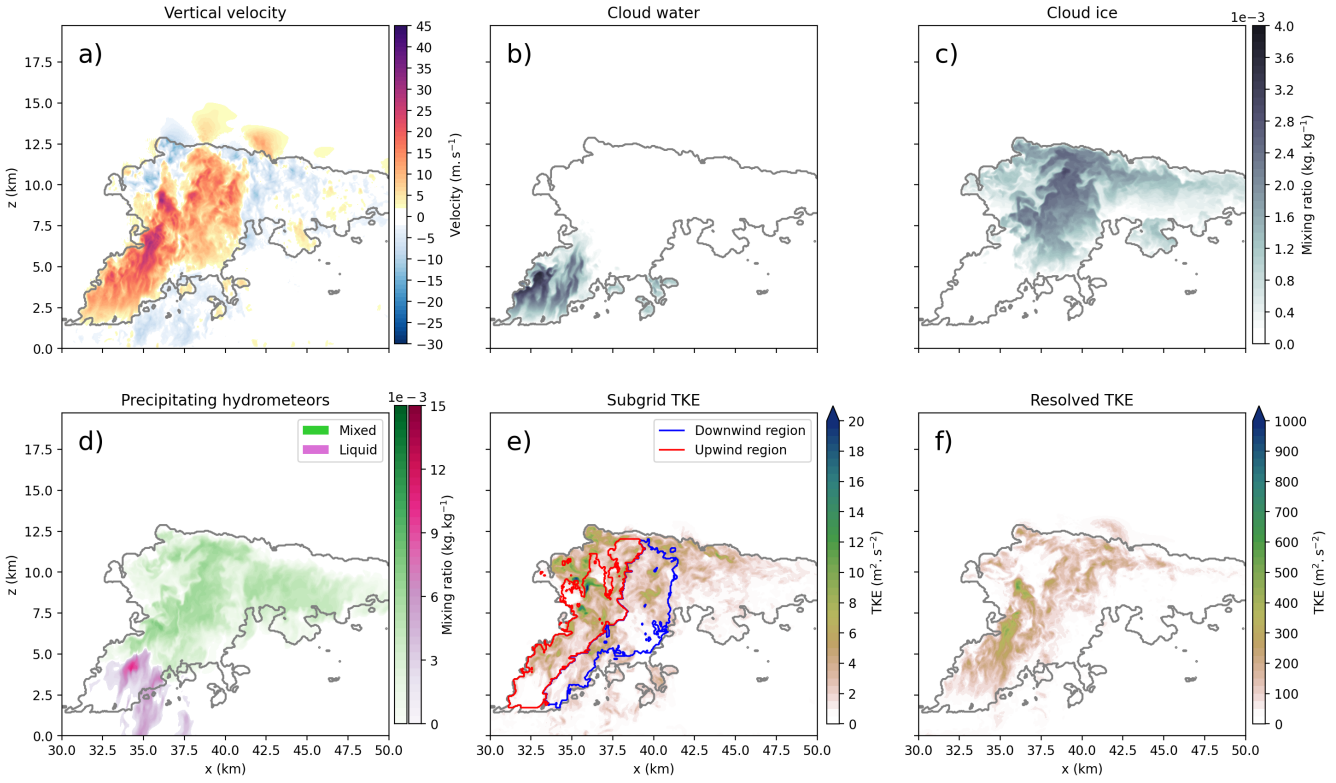


**Figure 2.** Vertical cross sections for simulation W10_S70 at 300 minutes. a) Vertical velocity~~and hydrometeor mixing ratios :~~ ; b) ~~cloud water,~~ and c) ~~cloud ice,~~ non precipitating hydrometeors mixing ratio; d) ~~rain,~~ precipitating hydrometeors mixing ratio; e) ~~snow~~ subgrid TKE with outlined upwind and downwind regions; and f) ~~graupel~~resolved TKE.

We first examine the simulations by computing the column-averaged vertical velocity over the domain (Figure 3). To highlight the correlation with the cloud cover, we overlay the cloud contour in grey. A grid point is classified as cloudy when the mixing ratio of cloud hydrometeors (the sum of cloud water and cloud ice) exceeds $1.10^{-6}$ kg/kg. ~~The cloud~~ A grid point is classified as part of an updraft core when it satisfies both the cloudy condition and a local vertical velocity exceeding 2 $\mathrm{m.s^{-1}}$. Cloud contour corresponds to the horizontal projection of the total cloud mask (Appendix A).

From these diagnostics, we notice that weakly sheared simulations develop convective cores with smaller area and weaker updrafts. However, no systematic intensification can be seen when comparing the most strongly sheared simulations to intermediate ones.

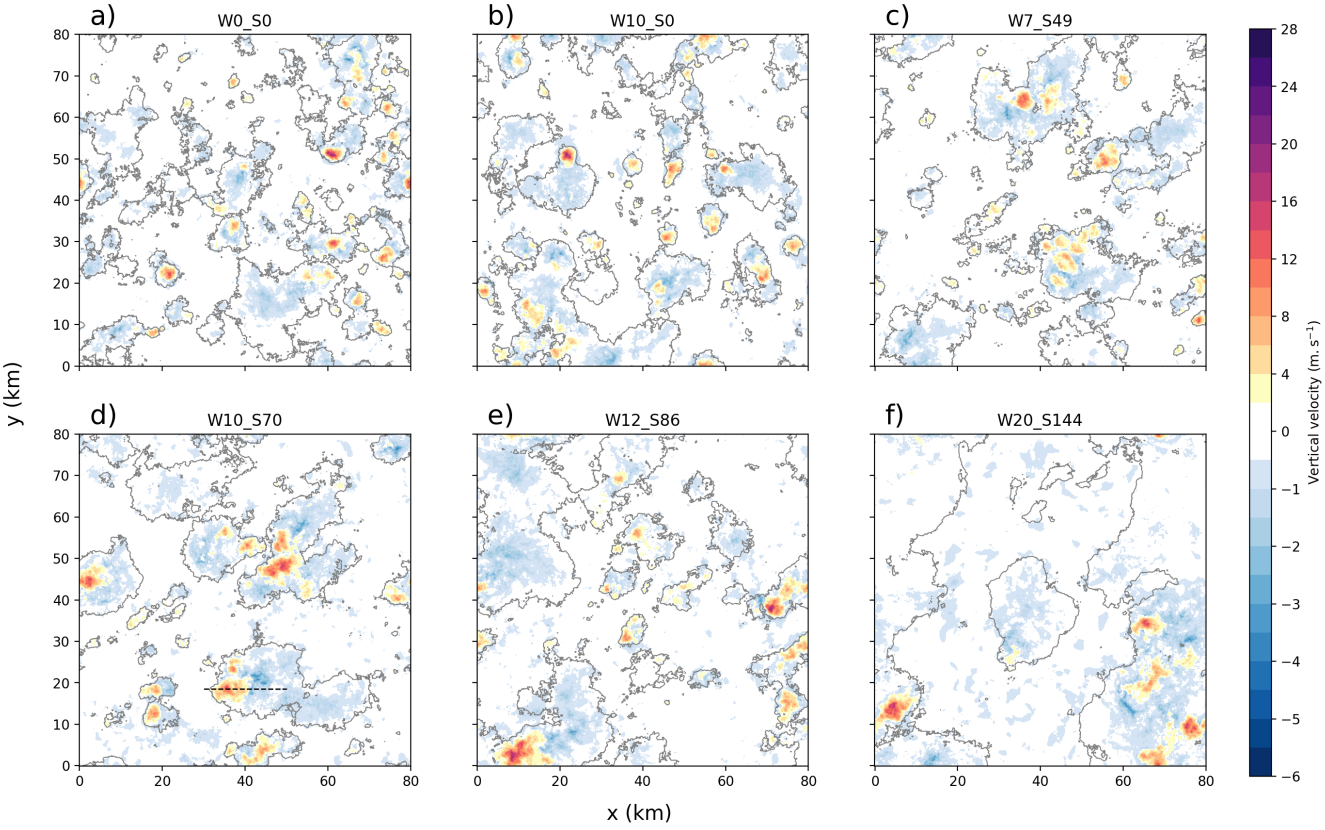


**Figure 3.** Column-averaged vertical velocity for several simulations at 300 minutes. Grey contour represents clouds. a) - f) correspond to different simulations.

To track the evolution of core intensity, we compute the mean vertical velocity in updraft cores over the whole domain at each output time (every 5 minutes). Figure 4 a shows that mean updraft velocity increases over time (up to 300 minutes) for all simulations except the two with the strongest shear. In those cases, the mean updraft velocity peaks around 200 minutes before decreasing. Updraft helicity (Figure 4 b) computed within the convective cores (Kain et al., 2008) shows the same behaviour, with the largest contrast between the two most strongly sheared simulations and the others occurring around 200 minutes. From

this, we isolate two study periods : 150-210 minutes and 240-300 minutes. The first one during the growth phase captures the energy maximum in the two most strongly sheared simulations, while the second one represents the final hour of convective development in the other simulations.

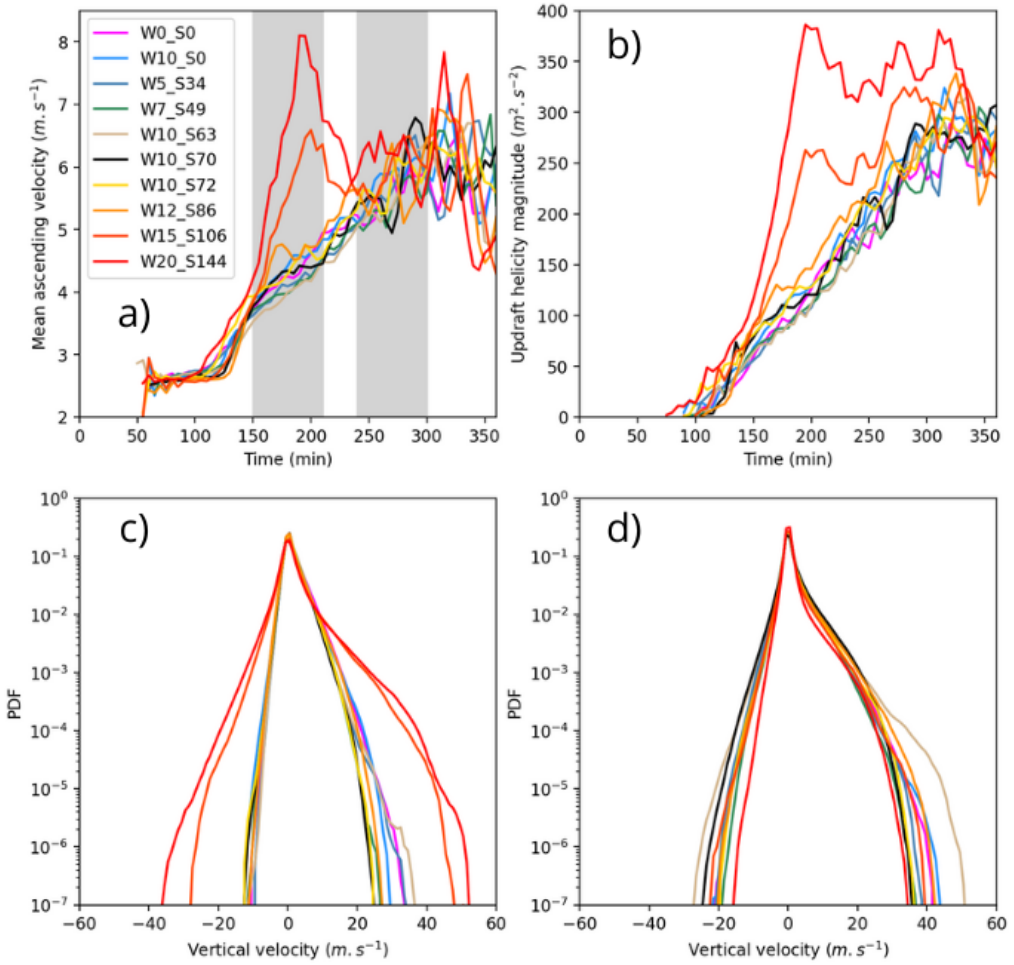


**Figure 4.** a) Evolution of ascending vertical velocity in updraft cores. b) Evolution of magnitude of updraft helicity in updraft cores. Distribution of vertical velocities in clouds, a) 150-210 minutes and b) 240-300 minutes.

For each of these two periods, we compute the distribution of vertical velocities inside clouds for all simulations (Figure 4 c and d). Between 150 and 210 minutes, the two most strongly sheared simulations show distributions with markedly larger extrema, whereas between 240 and 300 minutes, the other simulations have caught up, while ~~those two~~ W15_S106 and W20_S144 show diminished values.

To gain further insight, Figure 5 displays the column-averaged vertical velocity for simulation W20_S144 at 180, 190 and 200 minutes. A storm-splitting process occurs, producing a few large updraft cores with very strong vertical velocities. ~~The~~ These are reminiscent of supercells, which Markowski and Richardson (2001) characterize as convective storms with a

persistent and deep mesocyclone within the updraft. We used their definition of a mesocyclone as "a region of vertical vorticity with a characteristic width of 3-8 km and magnitude of $O(10^{-2})$ $s^{-1}$" to identify the storms in this simulation as supercells. However, the $O(10^{-2})$ $s^{-1}$ vertical vorticity threshold is not directly representative of the values found in simulations with decametric resolution, since the numerical calculation of spatial derivatives is strongly affected by grid spacing. To obtain comparable values, we averaged the vertical vorticity over moving horizontal boxes of 1 km by 1 km. The black contour in Figure 5 corresponds to a horizontal projection of the total mask (see Appendix A). We observe that the strong updrafts resulting from the storm-splitting process exceed the threshold, and fall within the characteristic 3-8 km width range. We also tracked the movement of these storms through the accumulated precipitation field over the domain (not shown), which revealed splitting trajectories angled relative to the mean wind direction after the separation point. Therefore, we can confidently identify these storms as supercells. The same behaviour is observed in simulation W15_S106 ~~. These supercells~~(not shown).

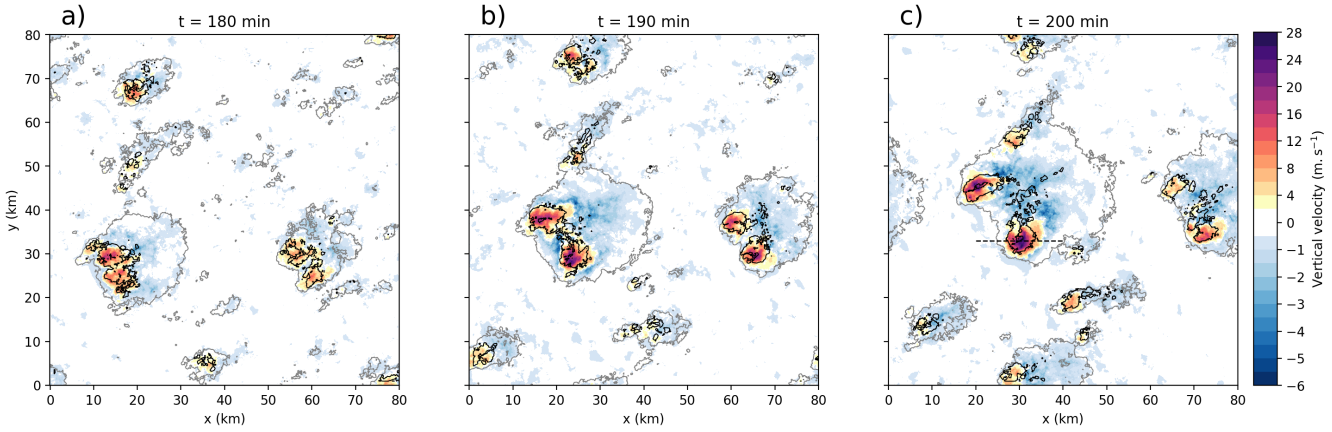


**Figure 5.** Column-averaged vertical velocity for simulation W20_S144 at different times. Grey contours represent clouds. Black contour represent the vertical vorticity threshold of $10^{-2}$ $s^{-1}$ Left to right : (a) 180 minutes, (b) 190 minutes, and (c) 200 minutes.

To provide a qualitative assessment of the supercells, we computed vertical cross-sections of one of them (Figure 6; the cross sections are indicated by the dashed line in Figure 5 c). Compared with the convective cell in Figure 2, the updraft is wider and less tilted, with stronger vertical velocities (up to 45 $m.s^{-1}$) and larger precipitating hydrometeors mixing ratios, all of which support the identification of these more intense storms as supercells. These structures correspond to the maxima in vertical velocity and updraft helicity shown in Figure 4 a) and b), which persist only briefly before dissipating. This is ~~confirmed in~~ further confirmed by Figure 3: at 300 minutes, the two most strongly sheared simulations no longer exhibit the large updraft cores present at 200 minutes, indicating that the convective systems have largely weakened by that ~~time~~stage.

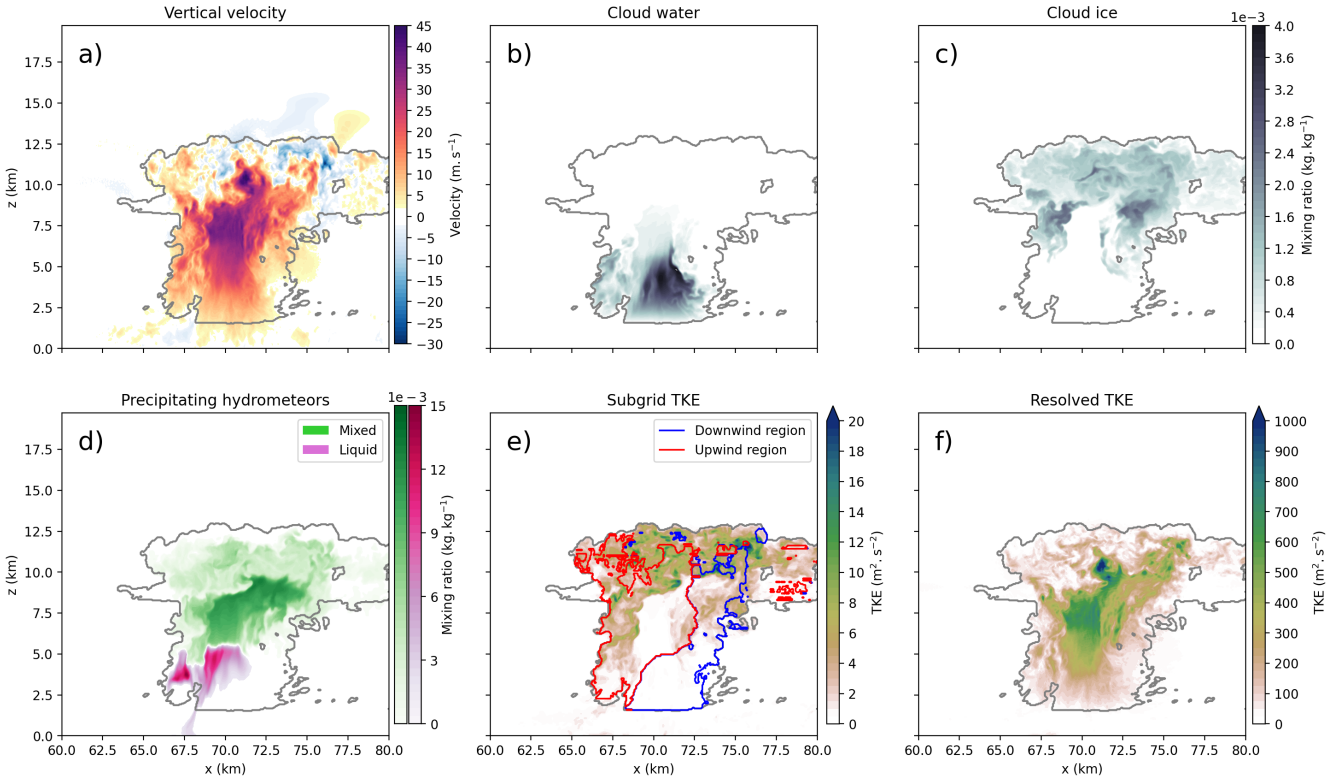


**Figure 6.** ~~Column-averaged vertical velocity~~ As in Figure 2 but for ~~simulation~~ W20_S144 at ~~different times. Grey contours represent clouds. Left to right : 180 minutes, 190 minutes and~~ 200 minutes.

Differences in storm regimes influence several associated phenomena. Regarding precipitation, we compute the domain-averaged accumulated precipitation. Its evolution reveals a robust trend of increasing precipitation with increasing wind shear (Figure 7 a), with a significant difference between the two most strongly sheared simulations and the others. After 6 hours, the supercell-producing simulations result in precipitation totals up to three times greater than the weakly-sheared ones. Correlating cloud volume with accumulated precipitation shows an excellent linear relationship across simulations at different time steps, although the slope varies with time. Because such correlations are often performed using cloud area and precipitation (Richards and Arkin, 1981), we also verified that cloud area and cloud volume are themselves well correlated (not shown).

Figure 7 c and d also presents the probability density functions (PDFs) of precipitation at 210 and 300 minutes for all simulations. At 210 minutes, both supercell-inducing simulations show much higher local precipitation amounts than all others. The windless case stands out from the weakly-sheared simulations, exhibiting locally heavier precipitation. This may result from convection initiation happening without inhibition from the shear and precipitating earlier, and from less mobile convective cells due to the absence of wind advection. By 300 minutes, the highest local precipitation amount is reached by W12_S86, the most strongly sheared simulations that does not produce supercells. The two supercell-producing simulations (W20_S144 and W15_S106) have been overtaken in terms of peak precipitation, although they still produce a larger number of moderately

high values (5-15 mm). The advection case W10_S0 stands out from all the others with much lower maximum precipitation, likely due to a more homogeneous spatial distribution.

~~a) Temporal evolution of mean accumulated precipitation. b) Correlation between cloud volume and accumulated precipitation across simulations at 210 and 300 minutes. PDF of accumulated precipitation for all simulations at 210 c) and 300 minutes d). e) Temporal evolution of the highest cloud-top altitude. Vertical profile of f) fractional entrainment and g) fractional detrainment at 300 minutes.~~

Since supercell-producing simulations develop convection earlier, differences in cloud-top height evolution are expected. To represent the maximum cloud extent more precisely, we compute the mean altitude of the (up to) 100 000 highest cloudy grid points (Figure 7 b). After a quick rise from 2 to 7 km AGL, with similar rates across all simulations, two regimes appear. The two supercell-producing simulations maintain a nearly constant rate of cloud-top ascent until a cap is reached around 12-13 km AGL, imposed by the tropopause. The other simulations show a strong reduction in ascent rate above 7 km, thereafter rising more slowly until reaching a cap around 12 km AGL. No internal differences appear clearly in this second group until reaching the maximum altitude. After 6 hours, all simulations exhibit capped cloud tops, but a trend remains: stronger shear corresponds to higher cloud tops.

However, since the initial CAPE is similar across simulations, the level of neutral buoyancy (LNB) estimated from the initial sounding should be the same in all cases. This difference between the estimated LNB and the simulated cloud-top height can be interpreted as a measure of entrainment dilution (Takahashi and Luo, 2012), as used in previous shear-related studies (Baidu et al., 2022 and Maybee et al., 2024). The reasoning is that the deficit in measured cloud top height stems from an energy loss during the ascent. This ~~is~~ could be caused by the dilution of cold and dry entrained air into the warm and moist air of the updraft, thereby reducing buoyancy. From this understanding, the higher cloud tops in more strongly sheared environments could indicate that their convective cores experience reduced entrainment dilution.

We ~~verified this by computing the~~ tried to verify this by estimating fractional entrainment and detrainment~~at 300 minutes for all simulations (Figure 7 e and f). Using the bulk-plum~~ . The bulk-plume method for offline computation, as described in Siebesma et al. (2003) and Dauhut et al. (2015), ~~we derive fractional entrainment and detrainment profiles. The conservative variable used is~~ is based on the assumption of a single, uniform updraft plume embedded in a homogeneous environment. The vertical variation of conservative variables within the plume is therefore entirely due to mixing between environmental and updraft air. From this hypothesis, a formulation for fractional entrainment is derived: $\epsilon = \frac{1}{\Phi_e - \Phi_u} \frac{\partial \Phi_u}{\partial z}$, which we applied using the total water mixing ratio as the conservative variable $\Phi$, both in the environment ($\Phi_e$) and within the updraft ($\Phi_u$). Fractional detrainment is then computed from the mass flux $M = \rho \overline{w} S$ with the hypothesis : $\delta = \epsilon - \frac{1}{M} \frac{\partial M}{\partial z}$. ~~As the~~

Using this method, we derive fractional entrainment and detrainment profiles at 300 minutes for all simulations (Figure 7 e and f). Since the computed profiles are very noisy, we ~~used~~ applied an exponential moving average over the model levels to ~~smoothen~~ smooth the data. The resulting profiles show a trend for more strongly sheared simulations to have lower fractional entrainment, with no trend on the detrainment. This is consistent with the ~~previous hypothesis of shear reducing entrainment dilution of the convective cores~~hypothesis from Mulholland et al. (2021), namely that shear reduces entrainment dilution within

convective cores, as well as with the findings of Abramian et al. (2023) regarding the effect of shear-modulated entrainment on precipitation.

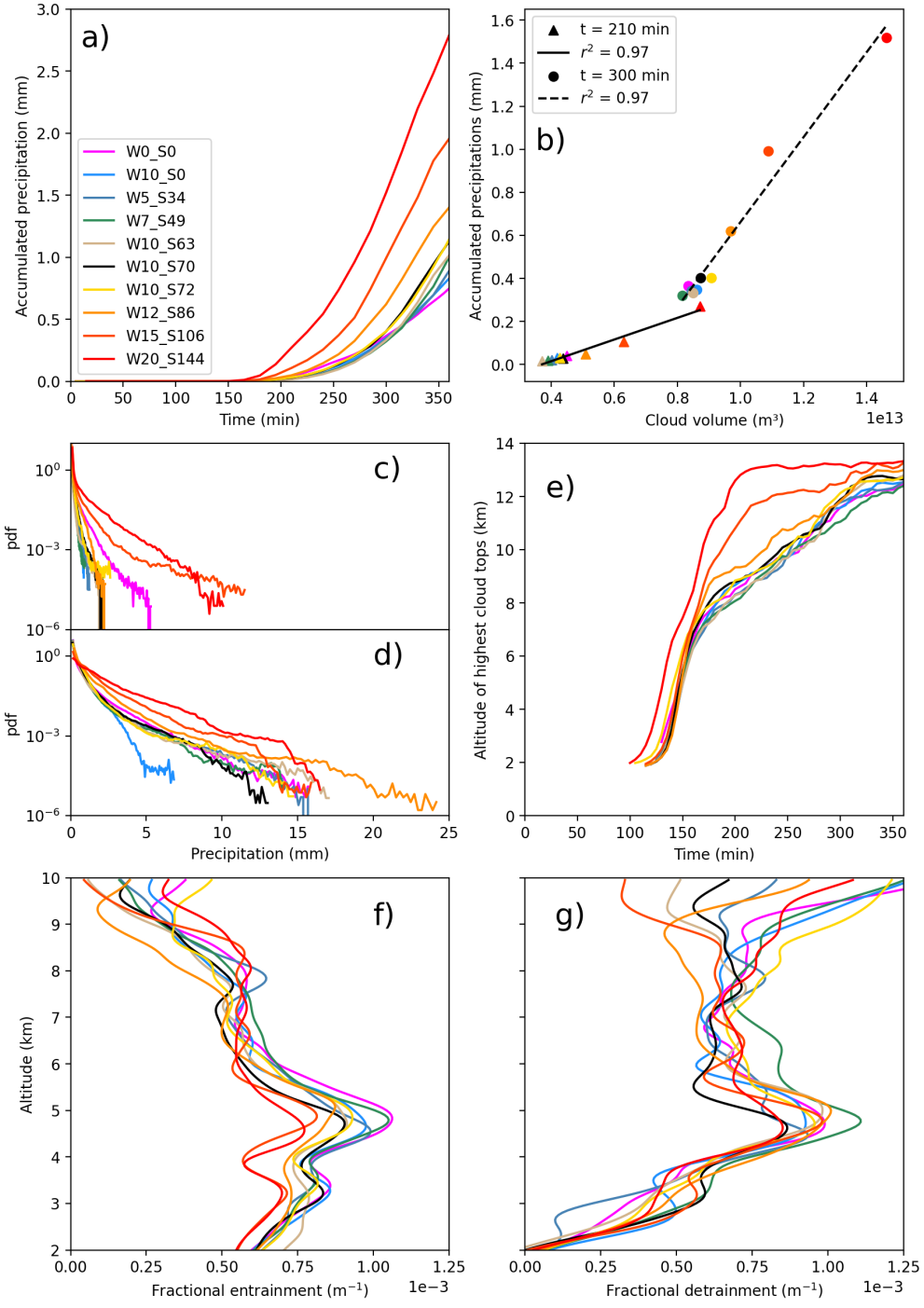


**Figure 7.** (a) Temporal evolution of mean accumulated precipitation. (b) Correlation between cloud volume and accumulated precipitation across simulations at 210 and 300 minutes. PDF of accumulated precipitation for all simulations at (c) 210 and (d) 300 minutes. (e) Temporal evolution of the highest cloud-top altitude. Vertical profile of (f) fractional entrainment and (g) fractional detrainment at 300 minutes.

To further investigate the mechanisms responsible for the differences in vertical velocity, we computed momentum budgets inside clouds (Figure 8). The advection term increases with shear in the updraft region. The gravity term also shows a clear increase with shear at 300 minutes within the updraft region. The pressure term exhibits values opposite in sign to those of the gravity term. At 210 minutes, the two supercell-producing simulations display a weaker gravity source term than at 300 minutes, with a corresponding opposite pressure contribution. Summing these three terms yields a vertical profile that is reasonably consistent with the resulting vertical acceleration profile. This profile shows a steady increase with shear, as well as more pronounced values for the supercell-producing simulations at 210 minutes.

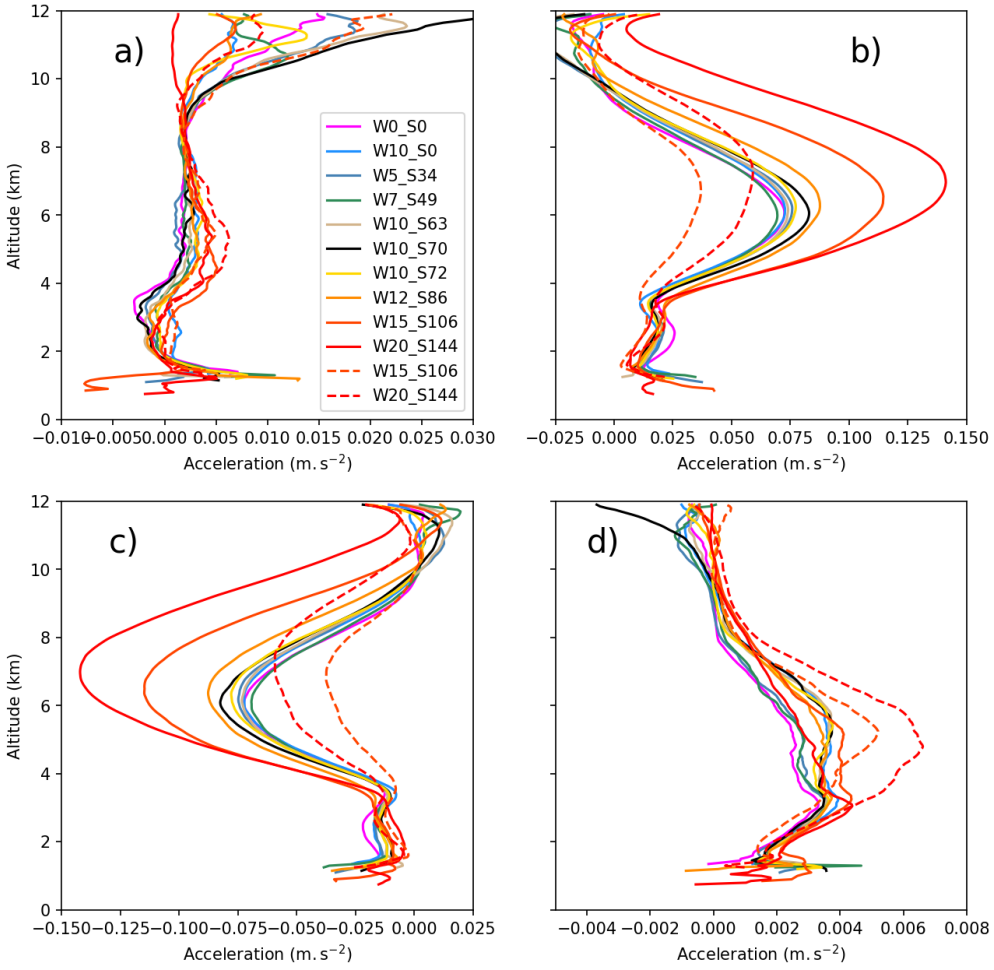


**Figure 8.** Vertical profiles of vertical momentum budget terms inside clouds at 300 minutes for all simulations (solid lines) and at 210 minutes for the two supercell-producing simulations (dashed lines): (a) advection term, (b) gravity term, (c) pressure term, and (d) the sum of the three previous terms.

### 3.2 TKE

We computed the resolved and subgrid turbulent kinetic energy (TKE) for the simulations. The subgrid TKE is a prognostic variable of the model, whereas the resolved TKE is computed from the velocity components via $e = \frac{1}{2}((\overline{u} - u)^2 + (\overline{v} - v)^2 + (\overline{w} - w)^2)$, with $\overline{u}$, $\overline{v}$ and $\overline{w}$ denoting the wind components averaged over each vertical level. These two values of TKE are then averaged over a time period (240-300 minutes), either on the whole domain or only within clouds. Since the number of cloudy grid points changes with time, the double averaging (over cloud area and over time) requires some care. We chose to represent the average TKE per grid point, normalised by the total number of cloudy points at each vertical level for the full time period. This means that the normalisation differs between vertical levels, but ensures that no cloud point is weighted higher than others due to the temporal variability. Note also that we set the TKE to zero at levels where cloud coverage fell below 3% of the domain, in order to reduce noise near the tropopause and ease interpretation. This does not affect values within the updraft.

Figure 9 shows differences in the resolved TKE in the updraft region (2-8 km AGL). A clear pattern emerges: more strongly sheared simulations exhibit higher resolved TKE, both within clouds and over the full domain. Subgrid TKE remains mostly the same for all simulations. As a result, the ratio of resolved to total TKE increases with shear and consistently exceeds 80%, supporting the classification of these experiments as LES (Pope, 2000). Because TKE is computed here for the 240-300 min time period, the two supercell-inducing simulations are already in a decaying stage, which explains some differences in the curve shapes. TKE values computed over the 150-210 minute time period are higher for these two cases (not shown).

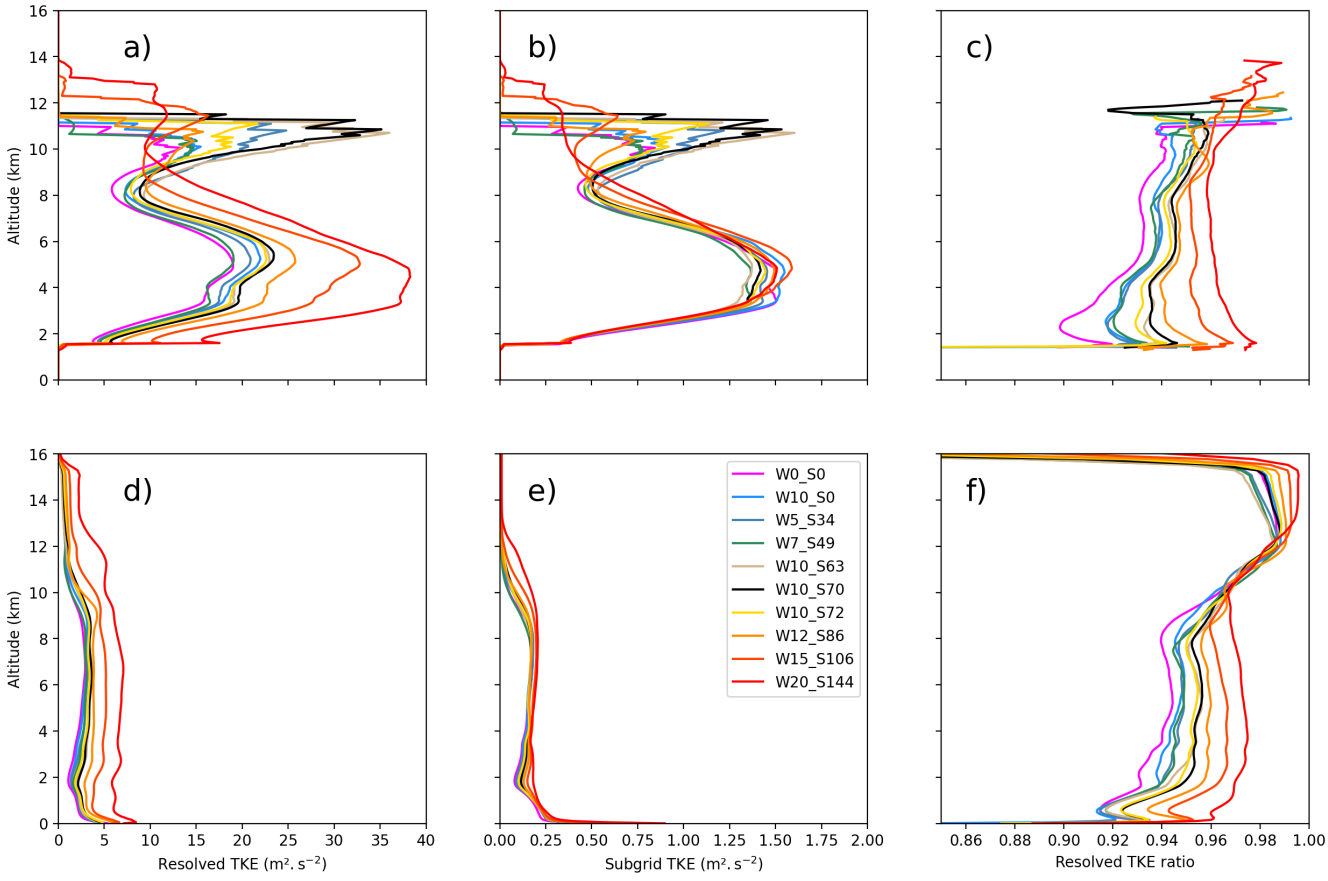


**Figure 9.** Averaged TKE profiles for all simulations between 240 and 300 minutes. First row within clouds, second row for the whole domain. Columns left to right : resolved TKE, subgrid TKE and ratio resolved/total.

In the lower levels, there is a peak in resolved dynamical production (not shown), linked to the increasing trend in wind shear. In the middle troposphere, resolved thermal production becomes the dominant source (not shown). The increase in resolved turbulence within the clouds is therefore consistent with the gravity term in the computed vertical momentum budget (Figure 8b).

We then investigated how ~~the turbulent quantities would~~ turbulent quantities vary between the upwind and downwind regions of the convective cores. A first indication of such an asymmetry was reported by Malkus (1949), who highlighted stronger turbulent motions upwind of cumulus clouds and downwind of cumulonimbus clouds within a turbulent wake. Using a dedicated mask that splits the convective cores into separated regions (Appendix B), we computed resolved and subgrid TKE over each mask, with the same normalisation method as above. Here, TKE was set to zero when the convective-core area represented less than 1% of the domain, to reduce noise at high altitude. This choice does not affect updraft values.

In Figure 10, all sheared simulations show systematically higher TKE on the upwind side (dashed lines) compared with the downwind side (solid lines), for both resolved and subgrid TKE, throughout the updraft region (2 - 8 km AGL). The

advected case (W10_S0), by contrast, displays almost no difference between upwind and downwind TKE. This is particularly noteworthy, as it suggests that the ~~asymetry~~ asymmetry depends on the presence of shear rather than on mean advection alone.

We also applied this diagnostic to the simulation without mean wind (W0_S0), but do not ~~to~~ show it here, as the definition of upwind and downwind regions hardly applies in that case.

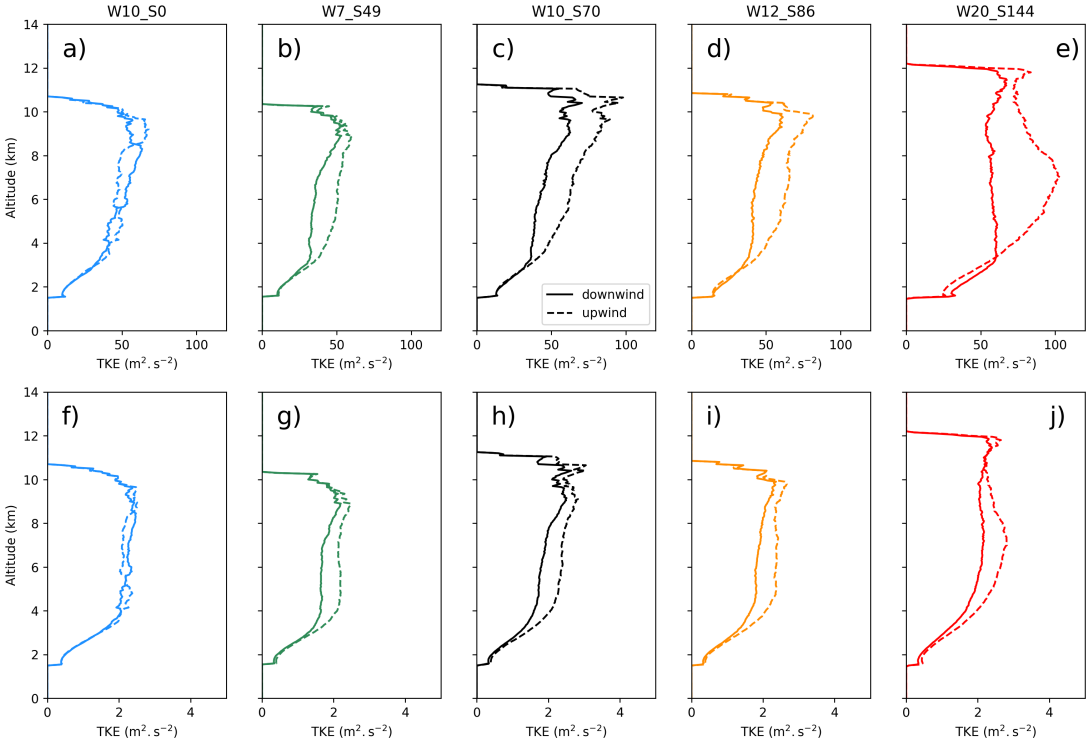


**Figure 10.** TKE profiles divided between upwind (dashed lines) and downwind (solid lines) region for several simulations between 240 and 300 minutes. For simulations W10_S0, W7_S49, W10_S70, W12_S86 and W20_S144, colour coded; a) - e) : resolved TKE; f) - j) : subgrid TKE.~~Dashed lines upwind, solid lines downwind.~~

We could expect the difference between upwind and downwind TKE to depend on wind parameters. To compare the magnitude of the asymmetry across simulations, we computed the relative difference $\Delta e_{u,d} = 2\frac{(e_u - e_d)}{(e_u + e_d)}$, for both resolved and subgrid TKE. As shown in Figure 11, no clear relationship can be drawn between shear intensity and the upwind/downwind TKE contrast. The two non-sheared simulations (W0_S0 and W10_S0) show very weak differences, and all the other simulations follow the same patterns, with relative differences reaching ~~up to~~ between 0.25 and 0.5 in the updraft region. One possible interpretation is that the TKE asymmetry stems from differences in velocity between the storm and the surrounding

flow, with storm motion speed being conditioned by the wind at its base. Shear may cause the environmental wind to exceed the storm motion, which could explain a higher TKE upstream of the convective cores. Another hypothesis, following Lasher-Trapp et al., 2021, would be that an asymmetric "P-shaped" circulation near cloud tops enhances entrainment differently on the upwind and downwind sides, thereby generating the observed TKE contrast.

This difference in TKE may appear inconsistent with the concept of a turbulent wake generated by convective cores acting as obstacles to the mean flow (Malkus, 1949 and Kingsmill and Wakimoto, 1991). However, because our analysis focuses on the updraft cores (as seen in Figure 2 e, f), potential wake regions may have been excluded, thereby allowing the detection of enhanced upwind TKE within the convective cores themselves.

Vertical (Figures 2 e-f, 6 e-f) and horizontal (non shown) cross-sections of TKE nevertheless confirm the presence of a turbulent wake downwind of the convective cores, mainly in the subgrid TKE field, although this wake appears less turbulent than the updraft cores.

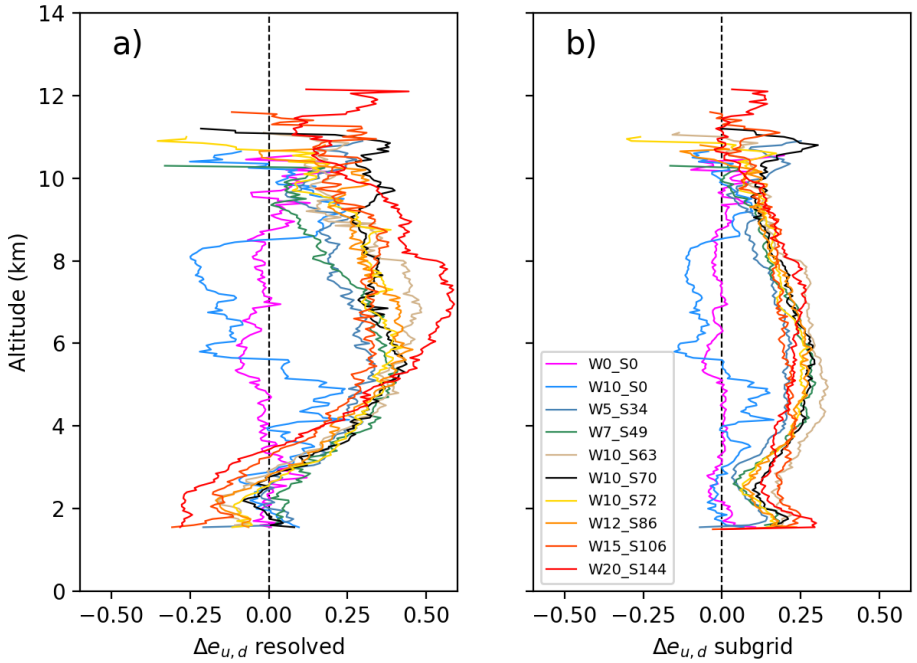


**Figure 11.** Relative difference between upwind and downwind TKE for all simulations. a) resolved TKE and b) subgrid TKE.

### 3.3 Cold pools

Convective systems commonly generate cold pools at the surface through the evaporation of raindrops. These cold pools can feed back ~~onto~~ into convection initiation, and are therefore of major interest for GCM parametrisation (Rio et al., 2009;

Grandpeix and Lafore, 2010) ~~. Typically, each convective core produces a single cold pool, and thus~~ and for the study of squall lines (Abramian et al., 2022). Abramian et al. (2023) showed that, for squall lines, an increase in shear intensity results in larger and deeper cold pools. We therefore expect that the observed variations in convective activity ~~affect~~ also affect the cold pool characteristics in our simulations. To visualise cold pools in the present simulations, we computed the virtual potential temperature $\theta_v$ at the first vertical level (25 m above the ground). Examining the anomaly of $\theta_v$ relative to its domain mean reveals the locations of cold pools (Figure 12). At first glance, more strongly sheared simulations produce larger and colder pools, but less numerous. We also note that negative $\theta_v$ anomalies are more prominent than positive ones. This motivates a more in-depth statistical analysis.

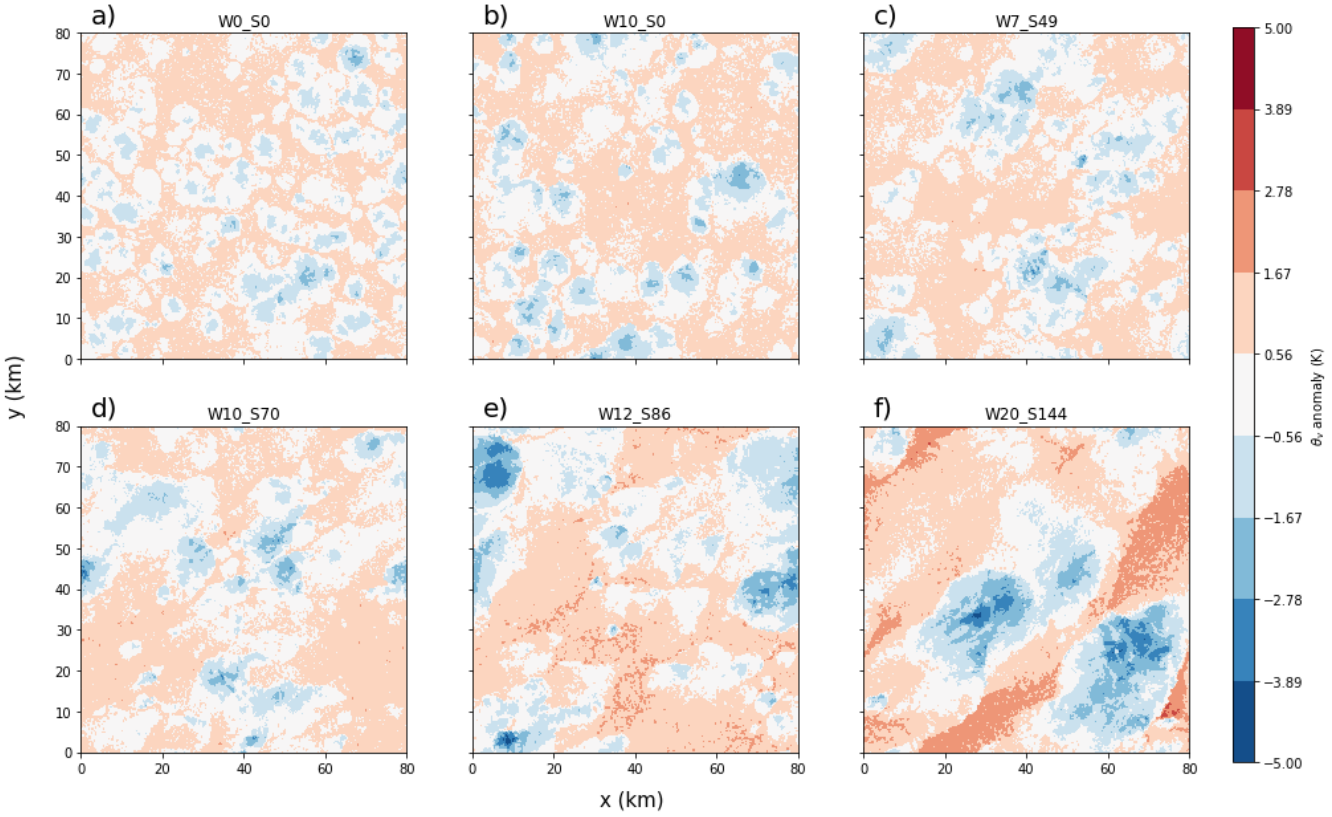


**Figure 12.** $\theta_v$ anomaly for several simulations at 300 minutes. a) - f) correspond to different simulations.

Considering the $\theta_v$ anomaly as a distribution, we can examine the evolution of its histogram over time in each simulation. In Figure 13, we observe that for all cases, the temperature at the first vertical level starts to increase (from light to dark colours), due to ~~the~~ surface fluxes. Since these fluxes are maintained throughout the entire simulation, it is important to note that ~~cold-pool~~ cold pool formation is dampened by this continuous surface heating, and existing cold pools are progressively eroded. After some time, cold pools begin to appear ~~,~~ and the distribution widens as the temperature decreases locally. Comparing the simulations, we find that the stronger the wind shear, the wider the distribution becomes.

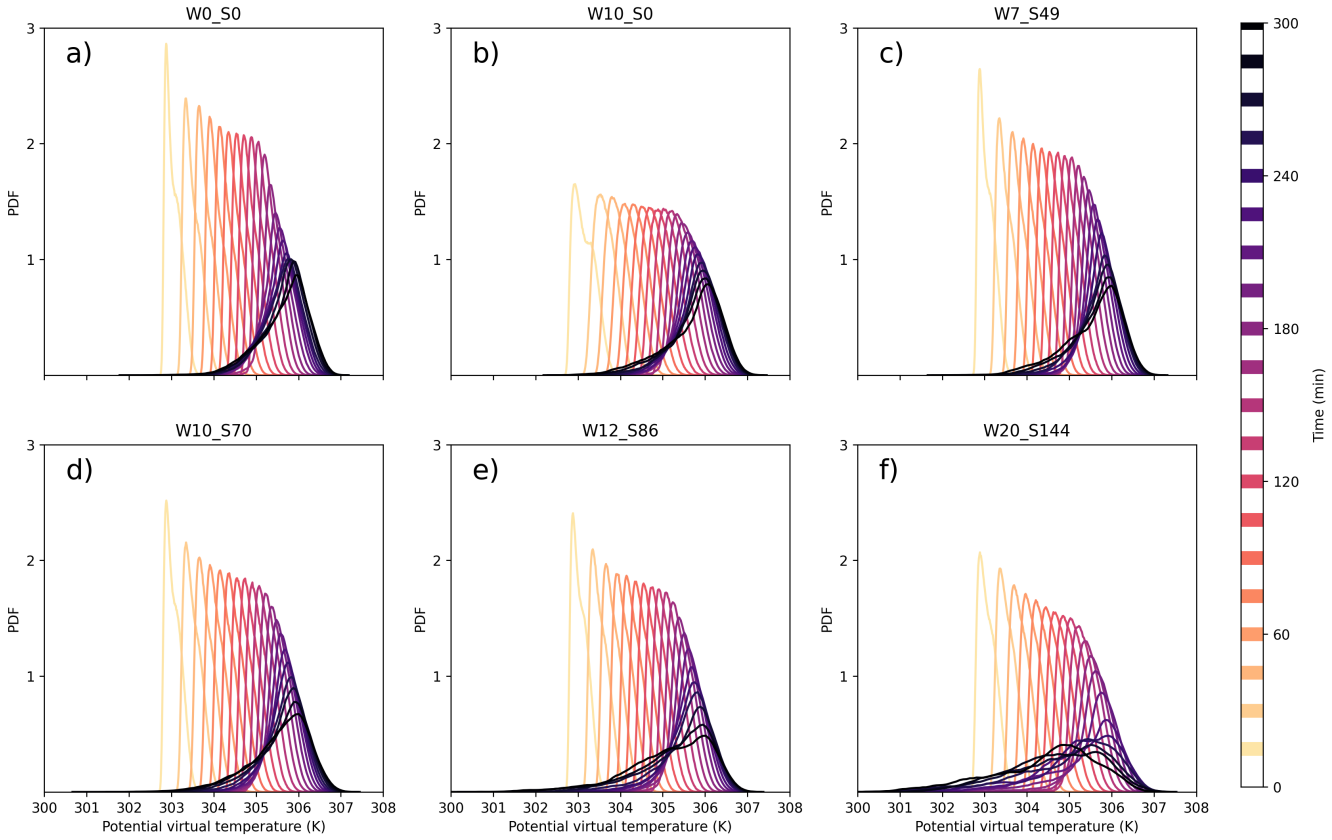


**Figure 13.** Evolution of $\theta_v$ distribution at the first vertical level for several simulations. On every panel, each line corresponds to a single timestep from the model, spanning every 15 minutes from 15 to 300 minutes following the colour coding described on the colourbar. Panels a) - f) show different simulations.

To better understand this asymmetry, we computed the temporal evolution of several statistical parameters. Computing the mean and median ~~for each histogram~~ of each histogram (Figure 14 a and b) reveals that, in most simulations, the formation of cold pools induces a divergence between these two metrics as the distribution becomes increasingly asymmetric. In the most strongly sheared cases, this asymmetry is accompanied by a ~~reduction~~ decrease in the average temperature: ~~surface air cools despite ongoing surface heating.~~

~~Evolution of $\theta_v$ distribution at the first vertical level for several simulations. a) - f) correspond to different simulations.~~

~~To better understand this asymmetry, we computed the temporal evolution of several statistical parameters.~~ the air in the first model level cools despite the ongoing surface fluxes. A side-by-side comparison of means and medians ~~for all the simulations (Figure 14 a and b)~~ emphasises the inclination for more strongly sheared simulations to cool the ~~surface~~ first model level more efficiently. The windless simulation behaves slightly differently from the others. With no wind or shear to inhibit convective initiation, the ~~surface~~ warming slows earlier than in the other simulations due to the first cold pools forming sooner. However, the very low energy convection is insufficient to compensate for the surface ~~heating~~fluxes, and the mean ~~surface temperature~~

temperature of the first level caps and stagnates. Regarding the shape of the distribution, the standard deviation (Figure 14 c) increases over time for all simulations, which acts as a proxy for the widening of the temperature distribution. A clear trend emerges: more strongly sheared simulations exhibit larger standard deviation and therefore broader distributions. Finally, examining the skewness of the distribution (Figure 14 d) reveals how the asymmetry evolves. Around the time cold pools begin to form, the distribution shifts from a slight positive skewness to a stronger negative skewness. The initial weak asymmetry is due to random perturbations in the initial conditions, and is quickly overwhelmed by the much stronger asymmetry induced by cold pools around 150 minutes. The two supercell-inducing simulations display the most noteworthy behavior, with a sharp surge in negative skewness coinciding with their energy spike, followed by a gradual decline.

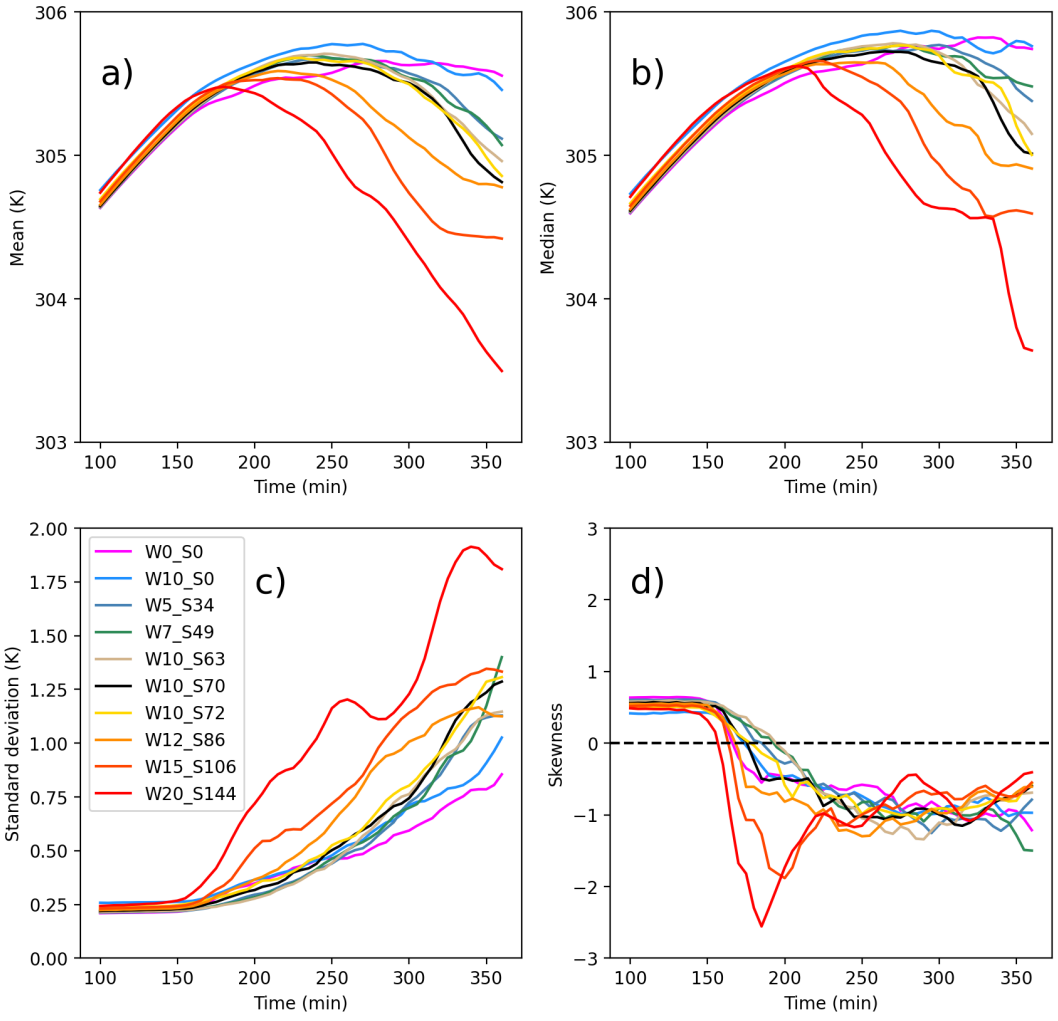


**Figure 14.** Temporal evolution of statistical parameters of the ~~surface~~ first vertical level virtual potential temperature $\theta_v$ for all simulations. a) - d) : mean, median, standard deviation and skewness.

### 3.4 Organisation

We hypothesise that many of the differences between our simulations can be related to differences in convective organisation. ~~However, verifying this requires to quantify objectively this organisation. This~~ We therefore attempt to measure such differences. Quantifying organisation is challenging, because its definition varies amongst studies (Tobin et al., 2012; White et al., 2018, Biagioli and Tompkins, 2023), and no consensus metric has yet emerged. Looking at the convective cores in Figures 5 and 3 suggests a first qualitative trend: more strongly sheared simulations present fewer convective cores, but these cores tend to be larger and more intense. We verified this by computing the number of updraft cores in each simulation (Figure 15 a). Starting from the mask of core points previously defined, we considered any two adjacent core points to belong to the same cluster, accounting for cyclic boundary conditions. This results in numerous core clusters, as isolated core points each form their own cluster. To reduce the influence of the smaller clusters, we computed two different quantities: the total number of core clusters, and the minimum number of cores required to represent 90 percent of the total core volume. The idea is to take into account only the significant core clusters, and to ignore the smallest ones. For this second metric, we observe a clear decrease in the number of updraft cores as shear increases (Figure 15 b), confirming the initial impression that more strongly sheared simulations contain fewer updraft cores.

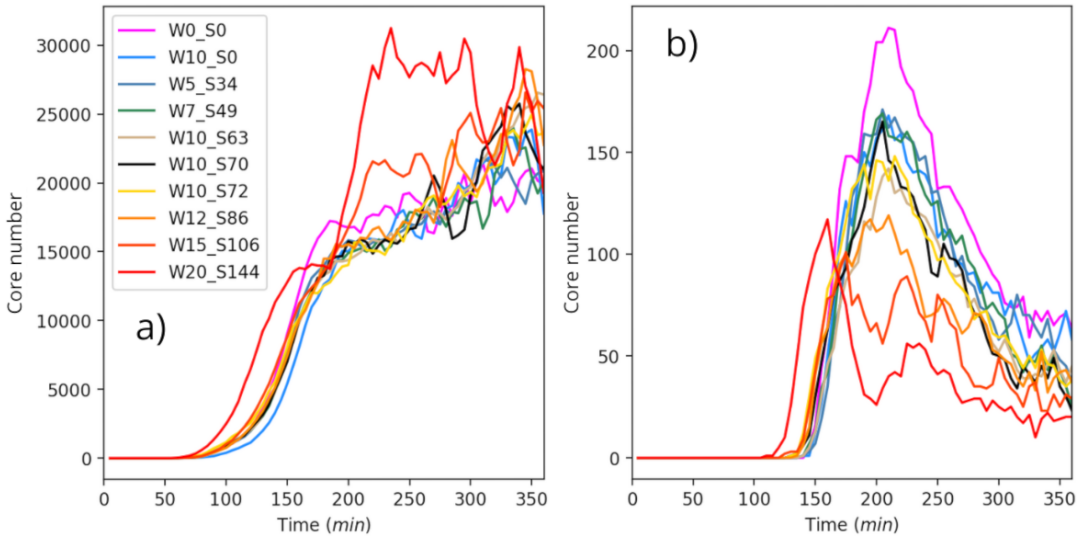


**Figure 15.** Temporal evolution of updraft core number for each simulation. a) total core number and b) minimum number of cores required to cover 90% of the total core volume at 300 minutes.

Although no single indicator of organisation has yet been isolated, several studies have attempted to narrow down the set of relevant metrics. Janssens et al., 2021 examined 21 different quantities previously used in the literature and applied a statistical reduction method to identify the four indicators that best represent the full set. These four indicators are : cloud-top altitude standard deviation, characteristic length, void size ratio (the ratio between the largest cloud-less rectangle in the domain and the domain size), and directional alignment, which we interpret here as eccentricity. Their method was applied to satellite images

of shallow convection, which differs markedly from our three-dimensional LES data. To address this limitation, we derived 2D cloud masks from our 3D fields ~~, and~~ by classifying a model column as "cloudy" when at least 30 grid points within the column exceed the $1.10^{-6}$ kg/kg threshold. The reasons for the choice of such a mask are detailed in Appendix A. We then applied the four selected indicators from Janssens et al. (2021) to ~~our simulations (Figure 16 )~~this mask of our simulations. Out of the four, we show in Figure 16 the three where trends appear. It is important to note that after 300 minutes, cloud cover has expanded across nearly the entire domain, erasing any meaningful differences between the simulations. Consequently, our analysis focuses on the 150-300 minute period.

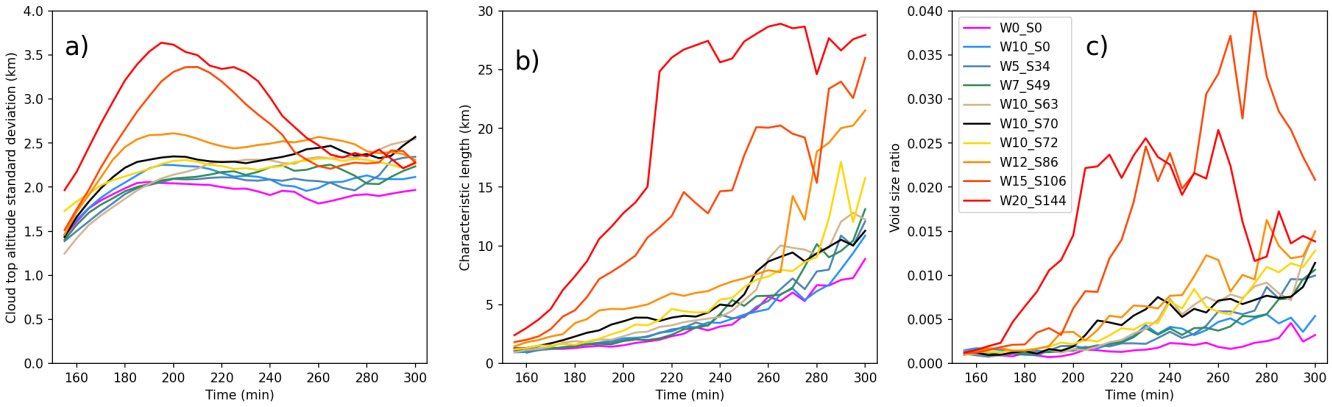


**Figure 16.** Temporal evolution of ~~4~~ 3 characteristic indicators for all simulations. a) - ~~d~~c) : cloud-top height standard deviation, cloud characteristic length ~~,~~ and void-size ratio~~and cloud eccentricity~~.

~~Tendencies appear on these graphs~~ A trend towards greater organisation with increasing shear appears in these graphs (Figure 16 a - c). The two most strongly sheared simulations clearly differ from the others across all indicators~~except eccentricity~~, exhibiting sharp peaks around their energy maximum at 200 minutes. The storm-splitting process, and the resulting supercells, induce strong variations in cloud radius, void sizes, and cloud-top height standard deviation~~(Figure 16 a - c)~~. Overall, strong wind shear generates supercells whose signatures can be quantified as marked differences in organisation according to these indicators.

Moreover, both the cloud-top height standard deviation and the void-size ratio increase monotonically with mean shear. This confirms our earlier qualitative impression, based on visual inspection and core-count diagnostics, that more strongly sheared simulations develop more organised convection.

## 4 Conclusion and Discussion

In this study, we used LES to investigate the impact of vertical wind shear on deep convective clouds. We conducted a set of simulations spanning a wide range of shear intensities, supplemented by a windless simulation and one with a uniform advective wind. All simulations develop convective storms, but two distinct regimes emerge. In the two most strongly sheared

simulations, supercells form through the storm-splitting process, while the other simulations only develop ordinary convective cells. Since supercells arise exclusively in the most strongly sheared cases, this process requires mean wind shear to exceed a threshold of approximately 10 $\mathrm{m.s^{-1}.km^{-1}}$.

Beyond these two different regimes, we highlight several robust trends in the structure and evolution of convective storms. As a general and qualitative principle, stronger shear produces more intense storms. This conclusion can be supported by multiple diagnostics.

- Precipitation increases markedly with shear. After 6 hours, the most strongly sheared simulation produces nearly four times as much domain-averaged precipitation as the least-sheared one. The distribution of precipitation is also affected by wind shear, with the windless and shearless simulations behaving as notable outliers.

- The two regimes are clearly distinguishable in cloud-top height and ascending speed. The cloud tops of supercells increase continuously to their maximum values, whereas the other simulations display two ascending phases with different ascent rates. After 6 hours, more strongly sheared simulations systematically produce higher cloud tops, consistent with reduced entrainment dilution. Early peaks in mean updraft speed also clearly identify the supercell-producing cases.

- ~~Resolved TKE within clouds increases steadily with shear. This is likely linked to stronger vertical velocity and results in a higher resolved turbulence ratio. Upwind TKE is about 25% greater than downwind TKE in sheared simulations, a ratio that remains almost constant across shear intensities. In contrast, the windless and shearless simulations exhibit negligible differences between upwind and downwind regions.~~

- Cold pools become larger, colder, and less numerous with increasing wind shear. The distribution of surface virtual potential temperature shows decreasing mean and median values, along with increasing standard deviation, as shear strengthens. This reflects more efficient surface cooling by cold pools. The distribution's skewness also reverses sign, with a pronounced negative spike in the supercell-inducing simulations.

- Convective organisation also varies systematically with shear. In agreement with cold pools, convective cores become larger and fewer as shear increases. Three of the four selected organisation indicators show clear trends with shear: the cloud-top height standard deviation, the characteristic length scale, and the void-size ratio all increase with stronger shear.

- Resolved TKE within clouds increases steadily with shear. This is likely linked to stronger vertical velocity and enhanced buoyancy fluxes, resulting in a higher fraction of resolved turbulence. Upwind TKE is about 25% greater than downwind TKE in sheared simulations, and this ratio remains nearly constant across shear intensities. In contrast, the windless and shearless simulations exhibit negligible differences between the upwind and downwind regions. This contrast in TKE within convective cores does not appear to contradict the presence of turbulent wakes downwind of the convective cores reported in previous studies.

These very fine-scale simulations support previous findings showing that convection becomes more organised as vertical wind shear increases.

Regarding the last point above, by focusing on turbulence within convective cores, we have shown that turbulence is stronger upstream than downstream of convective clouds, in contrast with previous studies that mainly emphasised wake turbulence. Although wake turbulence is also present in our simulations, it remains less pronounced than the turbulence found within the convective cores.

Our work has mainly focused on different diagnostics of convection rather than deeply analysing the physical mechanisms underlying the effect of shear on deep convective clouds. Recent hypothesis ~~suggest~~ suggests that low-altitude pressure "footprint" may help sustain updrafts (Peters et al., 2022b), while other studies have shown that, in the presence of pre-existing cold pools, an increase in shear ~~kinetical~~ kinetic energy enhances updraft velocity (Mulholland et al., 2021).

Our study of cold pools was limited to the virtual temperature at the first model level. In-depth analysis of the structure of cold pools could be achieved using object-based methods (Boeing, 2016 and Rochetin et al., 2021), which are used in some parametrisation of convective initiation (Rooney et al., 2022 and Dauhut et al., 2023). Applying these techniques here could improve our understanding of the relative positions of cold pools and updrafts, and help disentangle cause-and-effect relationships.

Our evaluation of the organisation relies on three metrics. Although Janssens et al. (2021) showed that these are fairly representative of several others, we could also have used other metrics commonly employed metrics, such as $I_{org}$, or more recent ones such as those based on the layer-lifting model of convection (Alfaro, 2017), which have been used to evaluate squall lines in LES studies Bickle et al. (2022).

Future studies will explore the use of a two-moment microphysical scheme, allowing the explicit representation of droplet and ice crystal size distributions, which may influence evaporation and mixing processes at cloud edges. Besides, simulations in this study were conducted without a radiation scheme. Including radiative cooling in future studies will allow us to investigate its influence on cloud-top processes and cloud-development speed. Finally, this study also provided synthetic cloud datasets to develop retrieval algorithms for the CLOUD visible imagers of the upcoming C3IEL mission (Dandini et al., 2022)~~)~~. This satellite mission will provide high-resolution observations on cloud-top evolution and ascent rates, which~~in turn~~ , in turn, will help validate and improve atmospheric models simulating deep convection.

## Appendix A: 2D cloud masks

Computing 2-dimensional cloud masks for 3-dimensional data required some considerations. The challenge consists in determining an appropriate condition for each model column to be classified as cloudy. We tried 3 different approaches, with increasing constraints, and compared the results.

The first approach was to be as large as possible: if any point of a column is cloudy, then the column is to be considered cloudy. We then introduced a total thickness condition, as in at least $n$ points of the column needed to be cloudy (we fixed $n = 30$, meaning at least 1500 m of cloud depth). Finally, we added a continuity condition, so that at least $n$ consecutive points

of the column needed to be cloudy, still with $n = 30$. Each approach is more restrictive than the previous one, yet all can be argued for.

We tried all 3 masks for the relevant diagnostics, and chose the one which highlighted the best the appearing trends. For all diagnostics except for the void-size ratio, we ended up choosing the total and discontinuous thickness condition. For the void-size ratio, the least restrictive mask showed better results, although the discussed observation was present for all 3 masks.

## Appendix B: Upwind/Downwind masks

To compute upwind and downwind turbulent quantities, we had to define a 3-dimensional upwind/downwind mask for the convective cores. Several ideas were attempted, we describe here the approach that produced the best results.

Extending the idea of upstream and downstream to a 3-dimensional field would require an analysis of the streamlines, which is non-trivial due to the turbulent nature of the flow. We therefore restricted the method to a 2-dimensional analysis at each vertical level. At a given level, convective cores were isolated using 2D clustering. For each cluster, every point was projected onto the axis defined by the mean horizontal wind direction at that level. We then defined an upwind and downwind part of each cluster by comparing the position of each point relative to the cluster mean.

Repeating this process for each 2D cluster of a vertical level, and for each vertical ~~levels~~ level creates a mask over the whole domain with upwind and downwind regions for each convective core, as seen in Figure A1. This mask was used to compute turbulent quantities in the upwind and downwind parts of convective cores.

## Appendix C: Simulation cost

Running these simulations comes at a substantial computational cost. Although access to MeteoFrance's Belenos supercomputer enables the production of such high-resolution LESs, we consider it important to be transparent regarding the resources required.

Each simulation ran for about 100 hours on 8000 cores distributed across 100 nodes, corresponding to about 5% of the supercomputer's capacity for this duration. Using the energy consumption data provided by Belenos, we estimated the monetary and environmental cost of the simulations. However, these data present large fluctuations with some unrealistic spikes. We therefore limited our analysis to averaging the reasonable values. The following calculations are therefore very rough estimates and should be treated as such.

The energy consumption amounts to a total just under 100 MWh for all runs, accounting for those that failed (estimated 30 failed or trial runs for 10 successful ones). Considering France's average yearly consumption of 2.2 MWh/person, producing our data required the energy consumed by more than 40 average French people over a year. With the government-regulated price per kWh for individuals in 2024 of 0.25 €/kWh, a first estimate of the monetary cost for our simulations is 25 k€. This could arguably be lower with corporate rates. The carbon footprint of electricity in France is evaluated by the government-owned RTE electricity transport network. Their data for 2023 show a carbon footprint of 32 g$CO2_{eq}$/kWh for produced electricity. Hence,

the estimation of 3.2 tons $CO2_{eq}$ emitted as a result of our computations. This could arguably be higher by taking into account the imported electricity from other European countries. A footprint of 3.2 tons represents about 150% of the 2.2 tons $CO2_{eq}$ individual emission targeted by France's High Council for Climate (HCC) by 2050 in order to limit the global warming to 1.5°C. It is noteworthy that 2023 was a record year for low-carbon electricity in France (RTE), and that the French energy mix is one of the least carbonated amongst European countries (Directorate-General for Energy (European Commission), 2024).

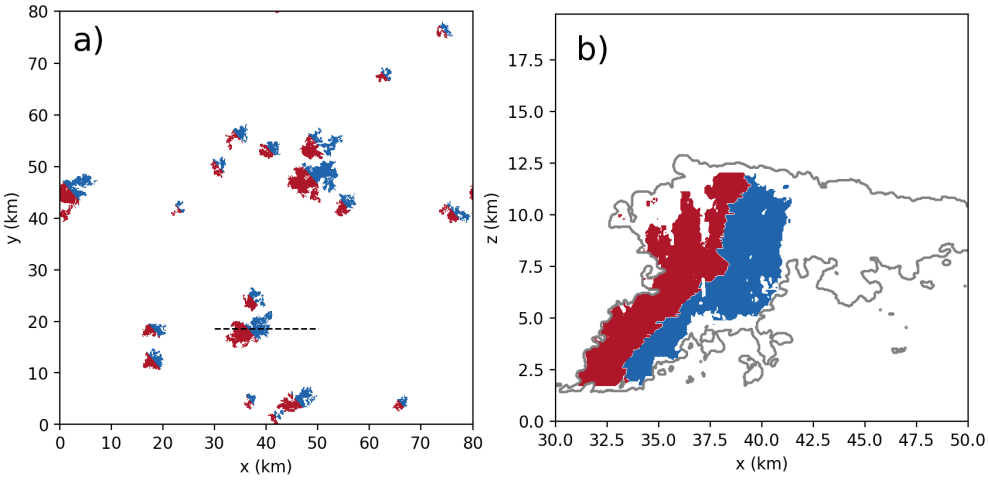


**Figure A1.** Mask of upwind (red) and downwind (blue) regions of convective cores for simulation W10_S70 at 300 minutes. a) horizontal ~~cross sections~~ cross-sections at $z = 6$ km and b) vertical slice at $y = 18.5$ km.

## References


Abramian, S., Muller, C., and Risi, C.: Shear-Convection Interactions and Orientation of Tropical Squall Lines, Geophysical Research Letters, 49, e2021GL095 184, https://doi.org/10.1029/2021GL095184, _eprint: https://agupubs.onlinelibrary.wiley.com/doi/pdf/10.1029/2021GL095184, 2022.

Abramian, S., Muller, C., and Risi, C.: Extreme Precipitation in Tropical Squall Lines, Journal of Advances in Modeling Earth Systems, 15, e2022MS003 477, https://doi.org/10.1029/2022MS003477, _eprint: https://agupubs.onlinelibrary.wiley.com/doi/pdf/10.1029/2022MS003477, 2023.

Alfaro, D. A.: Low-Tropospheric Shear in the Structure of Squall Lines: Impacts on Latent Heating under Layer-Lifting Ascent, Journal of the Atmospheric Sciences, 74, 229–248, https://doi.org/10.1175/JAS-D-16-0168.1, 2017.

Baidu, M., Schwendike, J., Marsham, J. H., and Bain, C.: Effects of vertical wind shear on intensities of mesoscale convective systems over West and Central Africa, Atmospheric Science Letters, 23, e1094, https://doi.org/10.1002/asl.1094, _eprint: https://onlinelibrary.wiley.com/doi/pdf/10.1002/asl.1094, 2022.

Biagioli, G. and Tompkins, A. M.: Measuring Convective Organization, Journal of the Atmospheric Sciences, 80, 2769–2789, https://doi.org/10.1175/JAS-D-23-0103.1, 2023.

Bickle, M., Marsham, J. H., Griffiths, S. D., Ross, A. N., and Crook, J.: The Influence of the Diurnal Cycle in Wind Shear and Thermodynamics on Squall Lines in the West African Monsoon, Journal of the Atmospheric Sciences, 79, 2125–2143, https://doi.org/10.1175/JAS-D-21-0025.1, 2022.

Boeing, S. J.: An object-based model for convective cold pool dynamics, Mathematics of Climate and Weather Forecasting, 2, 43–60, https://doi.org/10.1515/mcwf-2016-0003, number: 1, 2016.

Chen, X., Leung, L. R., Feng, Z., and Yang, Q.: Environmental Controls on MCS Lifetime Rainfall Over Tropical Oceans, Geophysical Research Letters, 50, e2023GL103 267, https://doi.org/10.1029/2023GL103267, _eprint: https://agupubs.onlinelibrary.wiley.com/doi/pdf/10.1029/2023GL103267, 2023.

Coffer, B. E. and Parker, M. D.: Impacts of Increasing Low-Level Shear on Supercells during the Early Evening Transition, Monthly Weather Review, 143, 1945–1969, https://doi.org/10.1175/MWR-D-14-00328.1, 2015.

Cuxart, J., Bougeault, P., and Redelsperger, J.-L.: A turbulence scheme allowing for mesoscale and large-eddy simulations, Quarterly Journal of the Royal Meteorological Society, 126, 1–30, https://doi.org/10.1002/qj.49712656202, _eprint: https://rmets.onlinelibrary.wiley.com/doi/pdf/10.1002/qj.49712656202, 2000.

Dandini, P., Cornet, C., Binet, R., Fenouil, L., Holodovsky, V., Y. Schechner, Y., Ricard, D., and Rosenfeld, D.: 3D cloud envelope and cloud development velocity from simulated CLOUD (C3IEL) stereo images, Atmospheric Measurement Techniques, 15, 6221–6242, https://doi.org/10.5194/amt-15-6221-2022, 2022.

Dauhut, T., Chaboureau, J.-P., Escobar, J., and Mascart, P.: Large-eddy simulations of Hector the convector making the stratosphere wetter, Atmospheric Science Letters, 16, 135–140, https://doi.org/10.1002/asl2.534, _eprint: https://rmets.onlinelibrary.wiley.com/doi/pdf/10.1002/asl2.534, 2015.

Dauhut, T., Couvreux, F., Bouniol, D., Beucher, F., Volkmer, L., Pörtge, V., Schäfer, M., Ayet, A., Brilouet, P.-E., Jacob, M., and Wirth, M.: Flower trade-wind clouds are shallow mesoscale convective systems, Quarterly Journal of the Royal Meteorological Society, 149, 325–347, https://doi.org/10.1002/qj.4409, _eprint: https://onlinelibrary.wiley.com/doi/pdf/10.1002/qj.4409, 2023.

Deardorff, J. W.: Stratocumulus-capped mixed layers derived from a three-dimensional model, Boundary-Layer Meteorology, 18, 495–527, https://doi.org/10.1007/BF00119502, 1980.

Directorate-General for Energy (European Commission): EU energy in figures: statistical pocketbook 2024, Office des publications de l'Union européenne, ISBN 978-92-68-16603-1, https://data.europa.eu/doi/10.2833/802460, 2024.

Doswell, C. A.: Severe Convective Storms, American Meteorological Society, 2001.

Durran, D. R.: Improving the Anelastic Approximation, Journal of the Atmospheric Sciences, 46, 1453–1461, https://doi.org/10.1175/1520-0469(1989)046<1453:ITAA>2.0.CO;2, 1989.

Goodman, S. J. and MacGorman, D. R.: Cloud-to-Ground Lightning Activity in Mesoscale Convective Complexes, Monthly Weather Review, 114, 2320–2328, https://doi.org/10.1175/1520-0493(1986)114<2320:CTGLAI>2.0.CO;2, 1986.

Grandpeix, J.-Y. and Lafore, J.-P.: A Density Current Parameterization Coupled with Emanuel's Convection Scheme. Part I: The Models, Journal of the Atmospheric Sciences, 67, 881–897, https://doi.org/10.1175/2009JAS3044.1, 2010.

Helfer, K. C. and Nuijens, L.: The Morphology of Simulated Trade-Wind Convection and Cold Pools Under Wind Shear, Journal of Geophysical Research: Atmospheres, 126, e2021JD035 148, https://doi.org/10.1029/2021JD035148, _eprint: https://onlinelibrary.wiley.com/doi/pdf/10.1029/2021JD035148, 2021.

Helfer, K. C., Nuijens, L., de Roode, S. R., and Siebesma, A. P.: How Wind Shear Affects Trade-wind Cumulus Convection, Journal of Advances in Modeling Earth Systems, 12, e2020MS002 183, https://doi.org/10.1029/2020MS002183, _eprint: https://onlinelibrary.wiley.com/doi/pdf/10.1029/2020MS002183, 2020.

Janssens, M., Vilà-Guerau de Arellano, J., Scheffer, M., Antonissen, C., Siebesma, A. P., and Glassmeier, F.: Cloud Patterns in the Trades Have Four Interpretable Dimensions, Geophysical Research Letters, 48, e2020GL091 001, https://doi.org/10.1029/2020GL091001, _eprint: https://onlinelibrary.wiley.com/doi/pdf/10.1029/2020GL091001, 2021.

Kain, J. S., Weiss, S. J., Bright, D. R., Baldwin, M. E., Levit, J. J., Carbin, G. W., Schwartz, C. S., Weisman, M. L., Droegemeier, K. K., Weber, D. B., and Thomas, K. W.: Some Practical Considerations Regarding Horizontal Resolution in the First Generation of Operational Convection-Allowing NWP, Weather and Forecasting, 23, 931–952, https://doi.org/10.1175/WAF2007106.1, 2008.

Kingsmill, D. E. and Wakimoto, R. M.: Kinematic, Dynamic, and Thermodynamic Analysis of a Weakly Sheared Severe Thunderstorm over Northern Alabama, Monthly Weather Review, 119, 262–297, https://doi.org/10.1175/1520-0493(1991)119<0262:KDATAO>2.0.CO;2, 1991.

Kirkpatrick, J. C., McCaul, E. W., and Cohen, C.: The Motion of Simulated Convective Storms as a Function of Basic Environmental Parameters, Monthly Weather Review, 135, 3033–3051, https://doi.org/10.1175/MWR3447.1, 2007.

Klemp, J. B. and Wilhelmson, R. B.: Simulations of Right- and Left-Moving Storms Produced Through Storm Splitting, Journal of the Atmospheric Sciences, 35, 1097–1110, https://doi.org/10.1175/1520-0469(1978)035<1097:SORALM>2.0.CO;2, 1978.

Knupp, K. R. and Cotton, W. R.: Convective cloud downdraft structure: An interpretive survey, Reviews of Geophysics, 23, 183–215, https://doi.org/10.1029/RG023i002p00183, _eprint: https://agupubs.onlinelibrary.wiley.com/doi/pdf/10.1029/RG023i002p00183, 1985.

Lac, C.: Peut-on prévoir les orages de grêle ?, La Météorologie, pp. 34–37, https://doi.org/10.4267/2042/54334, 2014.

Lac, C., Chaboureau, J.-P., Masson, V., Pinty, J.-P., Tulet, P., Escobar, J., Leriche, M., Barthe, C., Aouizerats, B., Augros, C., Aumond, P., Auguste, F., Bechtold, P., Berthet, S., Bielli, S., Bosseur, F., Caumont, O., Cohard, J.-M., Colin, J., Couvreux, F., Cuxart, J., Delautier, G., Dauhut, T., Ducrocq, V., Filippi, J.-B., Gazen, D., Geoffroy, O., Gheusi, F., Honnert, R., Lafore, J.-P., Lebeaupin Brossier, C., Libois, Q., Lunet, T., Mari, C., Maric, T., Mascart, P., Mogé, M., Molinié, G., Nuissier, O., Pantillon, F., Peyrillé, P., Pergaud, J., Perraud, E., Pianezze, J., Redelsperger, J.-L., Ricard, D., Richard, E., Riette, S., Rodier, Q., Schoetter, R., Seyfried, L., Stein, J., Suhre, K., Taufour,

M., Thouron, O., Turner, S., Verrelle, A., Vié, B., Visentin, F., Vionnet, V., and Wautelet, P.: Overview of the Meso-NH model version 5.4 and its applications, Geoscientific Model Development, 11, 1929–1969, https://doi.org/10.5194/gmd-11-1929-2018, 2018.

Lascaux, F., Richard, E., and Pinty, J.-P.: Numerical simulations of three different MAP IOPs and the associated microphysical processes, Quarterly Journal of the Royal Meteorological Society, 132, 1907–1926, https://doi.org/10.1256/qj.05.197, _eprint: https://rmets.onlinelibrary.wiley.com/doi/pdf/10.1256/qj.05.197, 2006.

Lasher-Trapp, S., Jo, E., Allen, L. R., Engelsen, B. N., and Trapp, R. J.: Entrainment in a Simulated Supercell Thunderstorm. Part I: The Evolution of Different Entrainment Mechanisms and Their Dilutive Effects, Journal of the Atmospheric Sciences, 78, 2725–2740, https://doi.org/10.1175/JAS-D-20-0223.1, 2021.

LeBel, L. J. and Markowski, P. M.: An Analysis of the Impact of Vertical Wind Shear on Convection Initiation Using Large-Eddy Simulations: Importance of Wake Entrainment, Monthly Weather Review, 151, 1667–1688, https://doi.org/10.1175/MWR-D-22-0176.1, 2023.

Malkus, J. S.: Effects of wind shear on some aspects of convection, Eos, Transactions American Geophysical Union, 30, 19–25, https://doi.org/10.1029/TR030i001p00019, _eprint: https://agupubs.onlinelibrary.wiley.com/doi/pdf/10.1029/TR030i001p00019, 1949.

Markowski, P. and Richardson, Y.: Mesoscale Meteorology in Midlatitude, Royal Meteorological Society, 2001.

Maybee, B., Marsham, J. H., Klein, C. M., Parker, D. J., Barton, E. J., Taylor, C. M., Lewis, H., Sanchez, C., Jones, R. W., and Warner, J.: Wind Shear Effects in Convection–Permitting Models Influence MCS Rainfall and Forcing of Tropical Circulation, Geophysical Research Letters, 51, e2024GL110 119, https://doi.org/10.1029/2024GL110119, _eprint: https://onlinelibrary.wiley.com/doi/pdf/10.1029/2024GL110119, 2024.

Maybee, B., Bassford, J., Marsham, J. H., Lewis, H., Field, P., Klein, C., and Parker, D. J.: How sensitive are Sahelian mesoscale convective systems to cold-pool suppression?, Quarterly Journal of the Royal Meteorological Society, 151, e5032, https://doi.org/10.1002/qj.5032, _eprint: https://rmets.onlinelibrary.wiley.com/doi/pdf/10.1002/qj.5032, 2025.

Mazur, V. and Rust, W. D.: Lightning propagation and flash density in squall lines as determined with radar, Journal of Geophysical Research: Oceans, 88, 1495–1502, https://doi.org/10.1029/JC088iC02p01495, _eprint: https://agupubs.onlinelibrary.wiley.com/doi/pdf/10.1029/JC088iC02p01495, 1983.

Misumi, R., Divjak, M., Tanahashi, S., and Takeda, T.: A Numerical Study on the Formation of Organized Convective Storms: Part I. Formation Patterns of Long-Lasting Cells, Journal of the Meteorological Society of Japan. Ser. II, 72, 235–253, https://doi.org/10.2151/jmsj1965.72.2_235, 1994.

Moncrieff, M. W. and Green, J. S. A.: The propagation and transfer properties of steady convective overturning in shear, Quarterly Journal of the Royal Meteorological Society, 98, 336–352, https://doi.org/10.1002/qj.49709841607, _eprint: https://rmets.onlinelibrary.wiley.com/doi/pdf/10.1002/qj.49709841607, 1972.

Morrison, H., van Lier-Walqui, M., Fridlind, A. M., Grabowski, W. W., Harrington, J. Y., Hoose, C., Korolev, A., Kumjian, M. R., Milbrandt, J. A., Pawlowska, H., Posselt, D. J., Prat, O. P., Reimel, K. J., Shima, S.-I., van Diedenhoven, B., and Xue, L.: Confronting the Challenge of Modeling Cloud and Precipitation Microphysics, Journal of Advances in Modeling Earth Systems, 12, e2019MS001 689, https://doi.org/10.1029/2019MS001689, _eprint: https://agupubs.onlinelibrary.wiley.com/doi/pdf/10.1029/2019MS001689, 2020.

Muetzelfeldt, M. R., Plant, R. S., Christensen, H. M., Zhang, Z., Woollings, T., Feng, Z., and Li, P.: Environmental Conditions Affecting Global Mesoscale Convective System Occurrence, Journal of the Atmospheric Sciences, 82, 391–407, https://doi.org/10.1175/JAS-D-24-0058.1, 2025.

Mulholland, J. P., Peters, J. M., and Morrison, H.: How Does Vertical Wind Shear Influence Entrainment in Squall Lines?, Journal of the Atmospheric Sciences, 78, 1931–1946, https://doi.org/10.1175/JAS-D-20-0299.1, 2021.

Pastushkov, R. S.: The effects of vertical wind shear on the evolution of convective clouds, Quarterly Journal of the Royal Meteorological Society, 101, 281–291, https://doi.org/10.1002/qj.49710142811, _eprint: https://rmets.onlinelibrary.wiley.com/doi/pdf/10.1002/qj.49710142811, 1975.

Peleg, N., Koukoula, M., and Marra, F.: A 2°C warming can double the frequency of extreme summer downpours in the Alps, npj Climate and Atmospheric Science, 8, 216, https://doi.org/10.1038/s41612-025-01081-1, 2025.

Peters, J., Hannah, W., and Morrison, H.: The Influence of Vertical Wind Shear on Moist Thermals, Journal of the Atmospheric Sciences, 76, https://doi.org/10.1175/JAS-D-18-0296.1, 2019.

Peters, J. M., Nowotarski, C. J., and Mullendore, G. L.: Are Supercells Resistant to Entrainment because of Their Rotation?, Journal of the Atmospheric Sciences, 77, 1475–1495, https://doi.org/10.1175/JAS-D-19-0316.1, 2020.

Peters, J. M., Coffer, B. E., Parker, M. D., Nowotarski, C. J., Mulholland, J. P., Nixon, C. J., and Allen, J. T.: Disentangling the Influences of Storm-Relative Flow and Horizontal Streamwise Vorticity on Low-Level Mesocyclones in Supercells, Journal of the Atmospheric Sciences, 80, 129–149, https://doi.org/10.1175/JAS-D-22-0114.1, 2022a.

Peters, J. M., Morrison, H., Nelson, T. C., Marquis, J. N., Mulholland, J. P., and Nowotarski, C. J.: The Influence of Shear on Deep Convection Initiation. Part I: Theory, Journal of the Atmospheric Sciences, 79, 1669–1690, https://doi.org/10.1175/JAS-D-21-0145.1, 2022b.

Pinty, J.-P. and Jabouille, P.: A mixed-phase cloud parameterization for use in mesoscale non-hydrostatic model: Simulations of a squall line and of orographic precipitations., in: Conference on Cloud Physics, 1998.

Pope, S. B.: Turbulent Flows, Cambridge University Press, 2000.

Prein, A. F., Liu, C., Ikeda, K., Trier, S. B., Rasmussen, R. M., Holland, G. J., and Clark, M. P.: Increased rainfall volume from future convective storms in the US, Nature Climate Change, 7, 880–884, https://doi.org/10.1038/s41558-017-0007-7, 2017.

Richards, F. and Arkin, P.: On the Relationship between Satellite-Observed Cloud Cover and Precipitation, Monthly Weather Review, 109, 1081–1093, https://doi.org/10.1175/1520-0493(1981)109<1081:OTRBSO>2.0.CO;2, 1981.

Rio, C., Hourdin, F., Grandpeix, J.-Y., and Lafore, J.-P.: Shifting the diurnal cycle of parameterized deep convection over land, Geophysical Research Letters, 36, https://doi.org/10.1029/2008GL036779, _eprint: https://onlinelibrary.wiley.com/doi/pdf/10.1029/2008GL036779, 2009.

Rochetin, N., Hohenegger, C., Touzé-Peiffer, L., and Villefranque, N.: A Physically Based Definition of Convectively Generated Density Currents: Detection and Characterization in Convection-Permitting Simulations, Journal of Advances in Modeling Earth Systems, 13, e2020MS002 402, https://doi.org/10.1029/2020MS002402, _eprint: https://onlinelibrary.wiley.com/doi/pdf/10.1029/2020MS002402, 2021.

Rooney, G. G., Stirling, A. J., Stratton, R. A., and Whitall, M.: C-POOL: A scheme for modelling convective cold pools in the Met Office Unified Model, Quarterly Journal of the Royal Meteorological Society, 148, 962–980, https://doi.org/10.1002/qj.4241, _eprint: https://rmets.onlinelibrary.wiley.com/doi/pdf/10.1002/qj.4241, 2022.

Rotunno, R. and Klemp, J.: On the rotation and propagation of simulated supercell thunderstorms, Journal of the Atmospheric Sciences, 1985.

Rotunno, R. and Klemp, J. B.: The Influence of the Shear-Induced Pressure Gradient on Thunderstorm Motion, Monthly Weather Review, 110, 136–151, https://doi.org/10.1175/1520-0493(1982)110<0136:TIOTSI>2.0.CO;2, 1982.

Schumacher, R. S. and Rasmussen, K. L.: The formation, character and changing nature of mesoscale convective systems, Nature Reviews Earth & Environment, 1, 300–314, https://doi.org/10.1038/s43017-020-0057-7, 2020.

Siebesma, A. P., Bretherton, C. S., Brown, A., Chlond, A., Cuxart, J., Duynkerke, P. G., Jiang, H., Khairoutdinov, M., Lewellen, D., Moeng, C.-H., Sanchez, E., Stevens, B., and Stevens, D. E.: A Large Eddy Simulation Intercomparison Study of Shallow Cumulus Convection, Journal of the Atmospheric Sciences, 60, 1201–1219, https://doi.org/10.1175/1520-0469(2003)60<1201:ALESIS>2.0.CO;2, 2003.

Strauss, C., Ricard, D., Lac, C., and Verrelle, A.: Evaluation of turbulence parametrizations in convective clouds and their environment based on a large-eddy simulation, Quarterly Journal of the Royal Meteorological Society, 145, 3195–3217, https://doi.org/10.1002/qj.3614, _eprint: https://onlinelibrary.wiley.com/doi/pdf/10.1002/qj.3614, 2019.

Takahashi, H. and Luo, Z.: Where is the level of neutral buoyancy for deep convection?, Geophysical Research Letters, 39, https://doi.org/10.1029/2012GL052638, _eprint: https://onlinelibrary.wiley.com/doi/pdf/10.1029/2012GL052638, 2012.

Thompson, R. L., Mead, C. M., and Edwards, R.: Effective Storm-Relative Helicity and Bulk Shear in Supercell Thunderstorm Environments, Weather and Forecasting, 22, 102–115, https://doi.org/10.1175/WAF969.1, 2007.

Tippett, M. K., Allen, J. T., Gensini, V. A., and Brooks, H. E.: Climate and Hazardous Convective Weather, Current Climate Change Reports, 1, 60–73, https://doi.org/10.1007/s40641-015-0006-6, 2015.

Tobin, I., Bony, S., and Roca, R.: Observational Evidence for Relationships between the Degree of Aggregation of Deep Convection, Water Vapor, Surface Fluxes, and Radiation, Journal of Climate, 25, 6885–6904, https://doi.org/10.1175/JCLI-D-11-00258.1, 2012.

Verrelle, A., Ricard, D., and Lac, C.: Sensitivity of high-resolution idealized simulations of thunderstorms to horizontal resolution and turbulence parametrization, Quarterly Journal of the Royal Meteorological Society, 141, 433–448, https://doi.org/10.1002/qj.2363, _eprint: https://onlinelibrary.wiley.com/doi/pdf/10.1002/qj.2363, 2015.

Weisman, M. L. and Klemp, J. B.: The Dependence of Numerically Simulated Convective Storms on Vertical Wind Shear and Buoyancy, Monthly Weather Review, 110, 504–520, https://doi.org/10.1175/1520-0493(1982)110<0504:TDONSC>2.0.CO;2, 1982.

Weisman, M. L. and Klemp, J. B.: The Structure and Classification of Numerically Simulated Convective Stormsin Directionally Varying Wind Shears, Monthly Weather Review, 112, 2479–2498, https://doi.org/10.1175/1520-0493(1984)112<2479:TSACON>2.0.CO;2, 1984.

Weisman, M. L., Klemp, J. B., and Rotunno, R.: Structure and Evolution of Numerically Simulated Squall Lines, Journal of the Atmospheric Sciences, 45, 1990–2013, https://doi.org/10.1175/1520-0469(1988)045<1990:SAEONS>2.0.CO;2, 1988.

White, B. A., Buchanan, A. M., Birch, C. E., Stier, P., and Pearson, K. J.: Quantifying the Effects of Horizontal Grid Length and Parameterized Convection on the Degree of Convective Organization Using a Metric of the Potential for Convective Interaction, Journal of the Atmospheric Sciences, 75, 425–450, https://doi.org/10.1175/JAS-D-16-0307.1, 2018.